

Tumor stem cells fuse with monocytes to form highly invasive tumor-hybrid cells

Luis Augusto Aguirre , Karla Montalbán-Hernández , José Avendaño-Ortiz , Elvira Marín , Roberto Lozano , Víctor Toledano , Laura Sánchez-Maroto , Verónica Terrón , Jaime Valentín , Elisa Pulido , José Carlos Casavilla , Carolina Rubio , Luke Diekhorst , Fernando Laso-García , Carlos del Fresno , Ana Collazo-Lorduy , Beatriz Jiménez-Munarriz , Paloma Gómez-Campelo , Emilio Llanos-González , María Fernández-Velasco , Carlos Rodríguez-Antolín , Rebeca Pérez de Diego , Ramón Cantero-Cid , Enrique Hernández-Jimenez , Enrique Álvarez , Rocío Rosas , Blanca dies López-Ayllón , Javier de Castro , Stefanie K. Wculek , Carolina Cubillos-Zapata , Inmaculada Ibáñez de Cáceres , Prudencio Díaz-Agero , María Gutiérrez Fernández , María Paz de Miguel , David Sancho , Leon Schulte , Rosario Perona , Cristóbal Belda-Iniesta , Lisardo Boscá & Eduardo López-Collazo


To cite this article: Luis Augusto Aguirre , Karla Montalbán-Hernández , José Avendaño-Ortiz , Elvira Marín , Roberto Lozano , Víctor Toledano , Laura Sánchez-Maroto , Verónica Terrón , Jaime Valentín , Elisa Pulido , José Carlos Casavilla , Carolina Rubio , Luke Diekhorst , Fernando Laso-García , Carlos del Fresno , Ana Collazo-Lorduy , Beatriz Jiménez-Munarriz , Paloma Gómez-Campelo , Emilio Llanos-González , María Fernández-Velasco , Carlos Rodríguez-Antolín , Rebeca Pérez de Diego , Ramón Cantero-Cid , Enrique Hernández-Jimenez , Enrique Álvarez , Rocío Rosas , Blanca dies López-Ayllón , Javier de Castro , Stefanie K. Wculek , Carolina Cubillos-Zapata , Inmaculada Ibáñez de Cáceres , Prudencio Díaz-Agero , María Gutiérrez Fernández , María Paz de Miguel , David Sancho , Leon Schulte , Rosario Perona , Cristóbal Belda-Iniesta , Lisardo Boscá & Eduardo López-Collazo (2020) Tumor stem cells fuse with monocytes to form highly invasive tumor-hybrid cells, *Oncoimmunology*, 9:1, 1773204, DOI: [10.1080/2162402X.2020.1773204](https://doi.org/10.1080/2162402X.2020.1773204)

To link to this article: <https://doi.org/10.1080/2162402X.2020.1773204>



© 2020 The Author(s). Published with license by Taylor & Francis Group, LLC.





View supplementary material 





Published online: 16 Jun 2020.



Submit your article to this journal 

 Article views: 2213

 [View related articles](#) 

 [View Crossmark data](#) 

Tumor stem cells fuse with monocytes to form highly invasive tumor-hybrid cells

Luis Augusto Aguirre^{a,b}, Karla Montalbán-Hernández^{a,b}, José Avendaño-Ortiz^{a,b,c}, Elvira Marín^{a,b}, Roberto Lozano^{a,b}, Víctor Toledano^{a,b,c}, Laura Sánchez-Maroto^{a,b}, Verónica Terrón^{a,b}, Jaime Valentín^{a,b}, Elisa Pulido^{a,b}, José Carlos Casavilla^{a,b}, Carolina Rubio^{a,b}, Luke Diekhorst^d, Fernando Laso-García^d, Carlos del Fresno^{id e}, Ana Collazo-Lorduy^f, Beatriz Jiménez-Munarriz^f, Paloma Gómez-Campelo^{a,b}, Emilio Llanos-González^{a,b}, María Fernández-Velasco^{a,g}, Carlos Rodríguez-Antolín^h, Rebeca Pérez de Diego^{a,i}, Ramón Cantero-Cid^{a,b}, Enrique Hernández-Jimenez^{a,b}, Enrique Álvarez^{a,b}, Rocío Rosas^h, Blanca dies López-Ayllón^{h,j,k}, Javier de Castro^h, Stefanie K. Wculek^e, Carolina Cubillos-Zapata^{a,b,c}, Inmaculada Ibáñez de Cáceres^h, Prudencio Díaz-Agero^l, María Gutiérrez Fernández^d, María Paz de Miguel^m, David Sancho^e, Leon Schulteⁿ, Rosario Perona^{h,j,k}, Cristóbal Belda-Iniesta^f, Lisardo Bosca^{a,g,j}, and Eduardo López-Collazo^{a,b,c}

^aThe Innate Immune Response Group, IdiPAZ, La Paz University Hospital, Madrid, Spain; ^bTumour Immunology Lab, IdiPAZ, La Paz University Hospital, Madrid, Spain; ^cCentre for Biomedical Research Network of Respiratory Diseases (CIBERES), Madrid, Spain; ^dDepartment of Neurology and Stroke Centre, Neuroscience and Cerebrovascular Research Laboratory, IdiPAZ, La Paz University Hospital, Autonomous University of Madrid, Madrid, Spain; ^eImmunobiology Laboratory, National Centre for Cardiovascular Research (CNIC), Madrid, Spain; ^fOncology Department, Research Foundation HM Hospitals, Madrid, Spain; ^gCentre for Biomedical Research Network, CIBER-CV, Madrid, Spain; ^hBiomarkers and Experimental Therapeutics in Cancer Group, IdiPAZ, La Paz University Hospital, Madrid, Spain; ⁱLaboratory of Immunogenetics of Human Diseases, IdiPAZ, Madrid, Spain; ^jLaboratory of Experimental Models of Human Diseases, Biomedical Research Institute CSIC/UAM, Madrid, Spain; ^kCentre for Biomedical Research Network, CIBERER, Madrid, Spain; ^lThoracic Surgery Service, IdiPAZ, La Paz University Hospital, Madrid, Spain; ^mCell Engineering Laboratory, IdiPAZ, La Paz University Hospital, Madrid, Spain; ⁿInstitute for Lung Research/iLung, Research Group “Rna-biology of Inflammation & Infection,” Philipps University, Marburg, Germany

ABSTRACT

The ‘cancer cell fusion’ theory is controversial due to the lack of methods available to identify hybrid cells and to follow the phenomenon in patients. However, it seems to be one of the best explanations for both the origin and metastasis of primary tumors. Herein, we co-cultured lung cancer stem cells with human monocytes and analyzed the dynamics and properties of tumor-hybrid cells (THC), as well as the molecular mechanisms beneath this fusion process by several techniques: electron-microscopy, karyotyping, CRISPR-Cas9, RNA-seq, immunostaining, signaling blockage, among others. Moreover, mice models were assessed for *in vivo* characterization of hybrids colonization and invasiveness. Then, the presence of THCs in bloodstream and samples from primary and metastatic lesions were detected by FACS and immunofluorescence protocols, and their correlations with TNM stages established. Our data indicate that the generation of THCs depends on the expression of CD36 on tumor stem cells and the oxidative state and polarization of monocytes, the latter being strongly influenced by microenvironmental fluctuations. Highly oxidized M2-like monocytes show the strongest affinity to fuse with tumor stem cells. THCs are able to proliferate, colonize and invade organs. THC-specific cell surface signature CD36⁺CD14⁺PANK⁺ allows identifying them in matched primary tumor tissues and metastases as well as in bloodstream from patients with lung cancer, thus functioning as a biomarker. THCs levels in circulation correlate with TNM classification. Our results suggest that THCs are involved in both origin and spread of metastatic cells. Furthermore, they might set the bases for future therapies to avoid or eradicate lung cancer metastasis.

ARTICLE HISTORY

Received 8 January 2020
Revised 14 April 2020
Accepted 10 May 2020

KEYWORDS

Cancer stem cells; CD36; lung cancer; metastasis; monocytes/macrophages

Introduction

According to The American Cancer Society, lung cancer is the leading cause of cancer-associated deaths.¹ Lung cancer is classified into small-cell (SCLC) and non-small-cell lung carcinoma (NSCLC). The latter accounts for more than 85% of cases and includes squamous-cell carcinoma, adenocarcinoma and large-cell carcinoma. Upon early detection, positive outcomes have improved during the last two decades using combinations of platinum-based drugs with radiotherapies, and an increase in life expectancy of more than 20 years has been achieved. However, a substantial proportion of patients – more than 65% – show tumor spread already at the time of diagnosis, and 40% of

NSCLC patients have distant metastases at presentation,² which makes the search for efficient personalized treatments difficult.

Following the ‘seed and soil’ theory, there exists an extended consensus in describing metastasis as a process by which lost tumor cells, mainly known as circulating tumor cells (CTCs)^{3,4} travel through the bloodstream and the lymphatic system, arrive at new “specific organs to their primary tumour,” settle, and either colonize it or remain in a quiescent state, known as disseminated tumor cells,^{5,6} until several other still unknown stimuli reactivate them to restart colonization. Though this theory has been deemed reliable in explaining the spread of cancer,⁷ it fails when accounting

for explanations on metastatic cells origin. Viz, the description sounds insufficient due to the presence of a high number of “obstacles” and checkpoints that cancer cells released from tumors would never be able to pass through on their own. Published data in the context of breast cancer indicate that CTCs can be reflective of the bulk of primary tumor biomass, but do not seem to generate metastases;⁸ moreover, to fully explain recent proof-of-concept of human-CTCs transmigration through mice blood-brain-barrier, researchers have postulated the active participation of microglia.⁹ In fact, most current drugs and clinical strategies designed to prevent metastasis have failed. Therefore, the grounds on which they are based might be incorrect. Probably, the only likely cells with required properties for this process, which include migration and evasion of immune defense, are immune system cells.

In this regard, the hypothesis that potentially metastatic cells are originated by leukocyte-tumor cell fusion has been taken into consideration during some intervals throughout the history of cancer research and then successively abandoned.¹⁰⁻¹² Most conclusive data reported are from several patients who received a bone marrow transplant: all had metastatic cells with DNA coming from the cancer-free donor.¹²⁻¹⁶ In addition to this clinical evidence, other authors have reported spontaneous hybridization between cells derived from bone marrow sarcomas,^{17,18} lymphoma,¹⁹ melanoma,²⁰ breast cancer^{21,22} and insulinoma,²³ availing the putative role for immune cells in this phenomenon. Apparently, myeloid cells are better equipped than tumor cells to mediate metastasis. After fused with tumor cells, resulting hybrids potentially acquire the information required for “tumour behaviour.”²⁴

Our data herein supports the notion that metastasis might be due to the fusion of myeloid cells with tumor stem cells, and shed light on the molecular mechanisms beneath this fusion, positioning CD36 scavenger-receptor as a key molecule on this process. A minor fraction of tumor cells with stemness hallmarks can specifically fuse with macrophages, even in a higher proportion than with other cancer cells. In this way, it is feasible for tumor cells to reach the bloodstream without any obstacles and to pass through checkpoints. Both figuratively and literally, it is a type of “Trojan horse” that, with a defense system appearance, brings tumor cells to remote sites to colonize other specific organs, in the form of new hybrid cellular entities, which we have therefore coined as tumor-hybrid cells (THCs), or Trojan horse cells.

Materials and methods

Human samples

All participants provided written informed consent in accordance with ethical guidelines of the 1975 Declaration of Helsinki and the Committee for Human Subjects of La Paz University Hospital (HULP: PI-3521) and the Clinical Research Ethics Committees of the Hospitals of Madrid (17.10.1125-GHM). Participants were grouped into healthy donors, septic or lung cancer patients. Buffy-coats from healthy anonymous donors were supplied by the Transfusion Center of the Community of Madrid.

Circulating nucleated cells were isolated after red blood cell lysis (BD Biosciences) of whole blood samples. PBMCs and plasma from buffy-coats were obtained by Ficoll-Plus gradient protocol.²⁵

Mice

Animals were properly housed in temperature- and light-regulated rooms with food and water *ad libitum*. All experimental designs followed the guidelines and were approved by the Ethics Committee for Animal Research from La Paz University Hospital (CSIC: 733/2018). Humane end-point criteria: suddenly required euthanasia prescribed due to impoverished physical conditions.

Cell lines

Human H460 and A549 NSCLC lines were purchased from ATCC and cultured in DMEM (Gibco) with 10% FBS, at 37°C in a humidified atmosphere with 5% CO₂. Puromycin-dependent (2.5 µg/mL) H460^{GFP} line was developed.²⁶ Cancer stem cells (CSCs) from H460/A549 were obtained by culture in non-treated Costar plates with selective DMEM/F-12 (Gibco, 1:1) with 2 mmol/L L-glutamine, 5 mmol/L HEPES, 0.4% bovine serum albumin, N-2 supplement (Gibco), 20 ng/mL of EGF (PeproTech) and 10 ng/mL bFGF (PeproTech).

A549 CD36-KO/wt pool, CRISPR-engineered for targeting the fourth exon of CD36, was purchased from Synthego. Clonal expansions were developed and tested for CD36 expression by PCR-Sanger sequencing (gDNA level), RT-qPCR (mRNA level) and western blot (protein level; sc-70644).

All reagents were endotoxin-free, as assayed with Limulus amoebocyte lysate test (Cambrex).

Genomic DNA isolation/amplification

Invitrogen kit (K1820-02) was used after scrapping seeded cells. *CD36* gene-targeted region surrounding exon 4 was amplified with 5'-GCC TTA AAA TCA ACA GTC GTG TCT-3' (forward) and 5'-AGA TTA GGA TTC TAT ACA GAC AGG AAA A-3' (reverse) primers. A 540 bp gDNA was sequenced by Sanger procedure using an ABIPrism3.1 sequencer.

Reverse-transcription qPCR

Total RNA was purified by using the High-Pure RNA isolation kit (Roche). Gene expression levels were assayed by using specific primers shown in Supplemental Table 1.

Western blot assays

Aliquots of 40 µg of protein (Bradford) from cells or vesicles lysates were electrophoresed on 10% SDS-PAGE gels, and proteins were transferred to 0.2 µm polyvinylidene fluoride membranes (Trans-Blot® Turbo™ Midi PVDF Transfer Packs; BIORAD-17041577). Then, primary and secondary antibodies incubations were performed, and the signal was detected by an Enhanced Chemiluminescent detection kit (BIORAD-17050622), followed

by autoradiography. Specific primary antibodies for each experiment are mentioned in corresponding sections.

Flow cytometry

Fluorescence-activated cell sorting (FACS) was performed using either BD Biosciences FACSCalibur/FACSCelesta/FACSCanto 3 L or Beckman-Coulter's Navios flow cytometers and raw data analyzed with FlowJo software (Tree Star). Sorting and cell collection were performed using either Synergy 2 L (Sony) or FACSaria II (BD Biosciences).

In vitro fusion assay protocol

Unless otherwise indicated, 1.8×10^5 /well PBMC-isolated monocytes from buffy-coats were routinely seeded (d_0) on tissue culture-treated Costar 24-well plates and allowed to adhere for 1 h (RPMI), PBS-washed and cultured (RPMI +10%FBS) for 16 h before adding CSCs (0.2×10^5 cells/well), thus starting d_1 of experimental fusion. Cells were recovered at d_5 by gentle tip-scraping, and measurement of surface markers expression by FACS was performed. Fused populations were assessed by gating $CD14^+GFP^+$ or $CD14^+PANK^+$ (PANK: Pan-cytokeratins; Miltenyi 130-080-101) double-positive cells.

In vivo invasiveness and migration assays

Twenty-four nu^-/nu^- female mice (Charles River, France) were i.v. inoculated with either 0.5×10^6 H460^{GFP}-CSC or $CD14^+GFP^+$ cells, and euthanized after 3, 6 or up to 28 weeks. Eighteen nu^-/nu^- female mice were inoculated with either $CD36^+CD14^+PANK^+$ or $CD36^-CD14^+PANK^+$ cells sorted from lung cancer patients' PBMCs, and let developing for up to 28 weeks.

Lungs, ganglia and spleens were extracted, and further IHC analysis for THCs was performed with anti-human CD14 (ab45870), PANK (ab9377) and CD36 (Miltenyi 130-108-018). Spleens were stained with haematoxylin/eosin and morphology injury average-scored (0-3), after pathologists' evaluation (ranging 0-3) of parameters:²⁷ i) minimized lymphoid follicles, ii) diffuse white pulp and distorted lymphoid architecture, iii) granular leukocytes in between lymphocytes in lymphoid follicles and iv) presence of giant macrophages. Thyroid transcription factor-1 expression was performed by IHC (TTF-1, DAKO-IR056) and percentage of the total area represented by dark-brown dots, calculated with ImageJ.

On the other hand, breast cancer 4T1 cells (10^5 in 50 μ L PBS each) or PBS alone as control were injected into the right 4th inguinal mammary gland of female BALB/c mice. Animals were monitored daily for tumor evolution. After 5 weeks, blood was collected from the submandibular vein and mice were sacrificed. Blood (100 μ L) was treated twice with Red Blood Cell Lysis Buffer (Sigma) for 5 minutes at RT. Remaining cells were stained in cold FACS buffer (PBS, 3% FBS, 1 mM EDTA) with a previous incubation with purified anti-Fc γ RIII/II (2.4G2, TONBO Bioscience) to block Fc-receptors. The cocktail of antibodies used included: α -CD45-PerPCy5.5, α -Ly6 C-PE, α -Ly6 G-BV450, α -CD11b-PECy7 (all from BD Biosciences) and α -Cytokeratin-8-Alexa Fluor

647 (Abcam). In all stains, dead cells were excluded by Hoechst 33258 (Invitrogen, Carlsbad, CA) incorporation, together with neutrophils (Ly6 G⁺ cells) to avoid their autofluorescence.

Measurement of circulating cells in human peripheral blood

BD FACS lysing solution (1 mL of 1X solution; BD Biosciences, Cat No. 349202) was added to 500 μ L of peripheral blood from lung cancer, aneurysm and septic patients, as well as controls, to lyse erythrocytes and preserve leukocytes. Tubes were thoroughly shaken at RT for 30 minutes, before washing twice with PBS. Resulting fixed leukocytes were assessed by FACS with the following human antibodies: CD14-PE, CD36-PerCP, CD45-APC-Cy7, EpCAM-APC and PANK-FITC. THCs (%) were gated as the $CD14^+$ population expressing CD36 and PANK, then $CD36^+CD14^+PANK^+$. This population was further assessed for the expression of CD45 and EpCAM, in order to compare them to CTCs ($CD45^-EpCAM^+$ population).

Organs and tumors immunohistochemistry

Tissues were fixed in 4% paraformaldehyde (SIGMA-P6148), embedded in OCT and cut into 10 μ m sections with a Leica RM2255 microtome (Leica Biosystems). The antibodies-stained sections were analyzed by confocal scanning laser microscopy, using a Leica SPE laser-scanning microscope (Leica Biosystems), and images quantified with ImageJ.

Tissue array immunohistochemistry

Two lung cancer *tissue microarrays* (TMAs) were purchased from Biomax (LC817a) and Abcam (ab178194). The former comprises primary tumor and lymph node metastasis whereas the latter is a tissue array of progressive lung cancer changes. They were stained for CD36 (Abcam, ab23680), CD14 (Abcam, ab133335) and PANK, and scored as negative (-) or positive (+) for CD36 or CD36/CD14/PANK by two researchers in a blind manner.

Vital colorant assays

DID/DIO protocol (Vybrant Multicolor Cell-Labeling kit, Fisher) experiments were conducted with human DID-monocytes faced to DIO-H460 CSCs, and DIO-H460-CSCs /DID-H460 cells competing for monocytes. Fluorescence emission of DID (665 nm, red) and DIO (501 nm, green) was assayed either by FACS or fluorescence microscopy.

Nuclei fusion assessment

Monocytes (1.8×10^5) from PBMCs were incubated with 10 nM EdU (Invitrogen-C10640) for 24 h, whereas H460^{GFP}-CSCs were incubated with 0.36 pM DAPI (ROCHE-10236276001) for 30 min, before co-cultures. After 5 days, cells were fixed in 3.7% formaldehyde (SIGMA-252549) and secondary Alexa-Fluor647 antibody was added (EdU, Invitrogen-C10640) and evaluated by confocal microscopy.

In vitro migration assay

Corning transwell chambers (8 μm , Sigma) were embedded or not with collagen (0.024% in RPMI w/o FBS). Co-cultures, monocytes and CSCs were scraped on d_5 into RPMI (w/o FBS) and seeded (10^5 cells) on the top compartment of transwell chambers; the bottom filled with 700 μL RPMI+10% FBS. After 48 h, top and bottom contents were recovered and cell migration (M) assessed as the percentage of each cell type in the bottom (B) with respect to the total amount seeded in the top compartment (A), according to: $M = [B/(A + B)] \times 100$. A control of 1000 inert beads (Reagent D from Mice CBA, BD Biosciences) was used to fit acquisition stop of sample collection during FACS.

In vitro proliferation assays

PBMCs (8.1×10^6) and H460-CSCs (0.9×10^6) were co-cultured for 5 days. After labeled, PANK⁺ tumor cells, CD14⁺ monocytes and PANK⁺CD14⁺ hybrids were sorted and a carboxyfluorescein succinimidyl ester (CFSE) proliferation assessment protocol was performed for each by FACS after 5 days.

Previous sorted cells (10^3 per well) were also co-cultured with CFSE-labeled PBMCs (2×10^4 per well) isolated from HVs. Immune phenotyping of T-cells was analyzed by FACS after 48 h; cytokines levels on supernatants were measured by cytometric bead array (BD CBA Human Th1/Th2/Th17 Cytokine Kit[™], BD Biosciences). After 5 days, T-cell proliferation induced by pokeweed mitogen (0.5 $\mu\text{g}/\text{mL}$) was also analyzed by FACS, in the presence/absence of 1 $\mu\text{g}/\text{mL}$ α -CD36 (Abcam, ab23680), α -CD39 (Biogend-328202), α -CD73 (Biogend-344002), α -PD-1 (Bristol-Myers Squibb) and 200 ng/mL α -Siglec5 (ThermoFisher PA5-47058) human antibodies.

Automated cell clustering was performed with the visNE algorithm available at Cytobank (www.cytobank.org).²⁸

Single hybrid cells growth monitoring

PANK⁺CD14⁺ labeled hybrid cells were sorted and each single cell seeded on cRPMI-filled wells of an ultra-low attachment (ULA) 96-wells plate. They were let to grow whilst periodic serial photos (Leica CTR6000) were taken throughout 20 days to register cells development. Eventually, *in vitro* tumors were disaggregated by thorough pipetting, and FACS analyzed for the expression of phenotyping epitopes with the following human antibodies: CD14-BUV395, CD45-PE-CF594, CD86-BUV737, HLA-DR-BV711, CD44-BV786, CD36-PerCP, PD-L1-BV421, EpCAM-BV605 and PANK-PE.

Cell imaging video-lapses

Monocytes (2×10^4 cells/well) were labeled with DID and cultured on a 1 μ -Slide 8 Well ibiTreat plate (ibidi, Germany). H460-CSCs (2×10^3 cells) were labeled with DIO, added to DID-monocytes, and plates placed on a Cell Observer[®] Z1 system (ZEISS) with standard culture conditions. Fifteen positions were selected randomly to take photos at an initial 5 min, and then in a 15 min interval during 72 h. Images were qualitatively analyzed using AxioVision LE 4.8.2.0 software (ZEISS).

A quantitative analysis of populations' dynamics and fusion kinetics was performed by seeding 1.8×10^5 DID-monocytes from three HVs and 2×10^4 DIO-H460-CSC cells, in a treated 24-well clear-film-bottom black plate (Eppendorf). Photos were taken every 20 min for the first 24 h, and every 90 min after to complete 120 h of video recording. Three fields per well were counted for red (DID⁺-monocytes)/green (DIO⁺-tumor cells)/tangerine (DID⁺DIO⁺-hybrids) dots with ImageJ.

In vitro myeloid-tumor cells fusion kinetics

Monocytes were grown for 15 days in order to check their developing to macrophages by specific antibodies: CD14-BUV395 (BD-563561), CD15-BV421 (BD-740086) and CD36-PerCP (Miltenyi-130 095 480). Simultaneously, the fusion event was followed-up with the above markers during the development process of both monocytes (d_0 to d_5) and macrophages (d_{10} to d_{15}).

Neutrophils were isolated from healthy donors using dextran protocol,²⁵ and their development and fusion affinity were followed-up for 5 days by specific markers: CD14-BUV395, CD15-BV421, CD16-BV480 (BD-566108), CD16b-PE (BD-550868), CD36-PerCP and CD66b-PE (Miltenyi-130 104 396).

NK cell expansion, activation and cytolytic activity

K562mbIL15-41BBL feeder cell line (10^7 cells) was co-cultured with 1.5×10^7 PBMCs for 2 weeks in stem cell growth medium (Cellgenix), with 10% human male AB serum (Sigma) to obtain highly purified NK cells. IL-2 (10 IU/mL) was added for the first week and 100 IU/mL thereafter. NK cells were then exposed to both sorted GFP⁺ and CD14⁺GFP⁺ cellular entities. After cell permeabilization (Cytotfix/Cytoperm kit, BD Biosciences), CD3⁻CD56⁺CD16⁺ NKs perforin generation was detected with specific Perforin-FITC (Miltenyi-130 096 668). Cytotoxicity was monitored with conventional 2 h Europium lysis-terpyridine dicarboxylic acid (TDA) release assay (Perkin-Elmer). NK (effector) cells loaded TDA-labeled (target) H460-CSC-GFP⁺ and CD14⁺GFP⁺ hybrid cells, at effector-to-target cell ratios of 50:1, 25:1, 12.5:1 and 6.25:1. Fluorescent measures (ex: 340 nm; em: 612 nm) were assessed in a BioTek Epoch Microplate Spectrophotometer.

Transmission electron microscopy (TEM)

After co-cultures sorting, cells were fixed with 1.5% glutaraldehyde in 0.1 M cacodylate buffer (pH 7.4) for 1 h at 4°C and then treated with 1% osmium tetroxide (in 0.1 M cacodylate buffer) and embedded in epoxy resin. Ultrathin sections were stained with uranyl-lead and examined in a JEOL JEM 1010 transmission electron microscope (JEOL USA, Inc., MA, USA).

RNA-Seq protocol and analysis

Stranded mRNA RNA-Seq libraries were prepared by Vertis Biotech (Freising-Weihenstephan, Germany) and sequenced on a NextSeq500 device (Illumina) with 75 bp read-length (single end). Base calling and demultiplexing were performed with RTA Version 2.4.11 and bcl2fastq Version 2.18.0.2, and reads were

mapped using the CLC genomics workbench with standard settings and the GRCh38 human reference annotation. The PCA analysis was carried out using the R-script prcomp (stats) and the rgl package based on row Z-scores of all mRNAs with a mean abundance \geq RPKM 1 in at least one cell type. Differentially expressed genes were identified using DESeq2 in R (padj \leq 0.001). Heatmaps were generated using JAVATreeView. Enriched Kyoto Encyclopedia of Genes and Genomes pathways (\geq 10 genes mapped per pathway) were identified using ConsensusPathDB with the gene set “over-representation” and “induced network modules” functions. RNA-Seq reads have been deposited in the NCBI-GEO (GSE102512).

Karyotype analysis

The three cell types (CD14⁺ monocytes, GFP⁺ H460^{GFP}-CSCs and CD14⁺GFP⁺ hybrids) were cultured according to standard techniques on culture slides and harvested. GTG banding was used for chromosome analysis. Images were analyzed on a Cytovision karyotyping system (Leica).

In vitro modulation of CD36 expression

Highly volatile 4HNE solution (64 mM, Merck) was quickly inoculated from -80°C storage into cRPMI-diluted CSCs, and added to seeded monocytes at final concentrations of 10, 20 and 40 μM , in order to chemically stimulate CD36 expression via *NRF2* enhancement in both cell types.

Commercial pUNO1-hCD36 (Nucliber) plasmid, hereafter pCD36, was used to perform independent transfections of each cell type. CSCs (7.5×10^5 per well) were transfected on d_{-1} with Lipofectamine-LTX (Invitrogen), hereafter Lipo, at a pCD36:Lipo ratio of 5 μg :12.5 μL diluted in 1 mL Opti-MEM (Gibco) and added to monocytes after 16 h. We assayed two different approaches to overexpress CD36 in monocytes: a) transfection (d_0) at a pCD36:Lipo ratio of 0.5 μg :1.25 μL diluted in 100 μL Opti-MEM per well; b) using Transfectosome[®] (Nanovex Biotechnologies SL, Spain) at a pCD36:Transfectosome ratio of 0.2 μg :0.6 μL diluted in Opti-MEM per well. A549 wt-CSCs and clone B10-CSCs, were also transfected with pCD36 following transfectosome protocol.

CD36 downregulation was evaluated with specific human CD36 siRNAs: (sense) CACUAUCAGUUGGAACAGAtt, (anti-sense) UCUGUCCAACUGAUAGUGaa; s2647 and 105938 from Ambion and α -CD36 antibody (ab133625), in HiPerFect reagent (Qiagen), hereafter HFT. CSCs (7.5×10^5 per well) were transfected with a (siRNA1+ siRNA2):HFT ratio of (2.5 μg +2.5 μg):12 μL . For monocytes, a (siRNA1 + siRNA2):HFT ratio of (0.5 μg +0.5 μg):6 μL diluted in cRPMI per well was used.

In vitro modulation of microenvironment and oxidation/polarization status

We used C11-BODIPY^{581/591} (ThermoFisher-D3861) 1 μM BODIPY (DMSO), hereafter called BODIPY, to measure the oxidative status of monocytes' membranes. For FACS analysis, samples were excited using a 488 nm laser, and fluorescence emission was collected with 530 nm (FL1) and 585 nm (FL2)

filters. An FL1/FL2 fluorescence quotient for oxidized/reduced BODIPY ratio was calculated.

Effects of oxLDL (ThermoFisher-L34357) and lactate (Sigma-07096) on both sole monocytes, and after they had been mixed with CSCs, were evaluated for 5 days. oxLDL was added on d_0 at 50 $\mu\text{g}/\text{mL}$. Lactate (24 mM) was added either at d_0 or for the last 16 h before the end of the experiment (d_5). CD163 (BD-556 018) was tested for M2-polarization status.

Standardized monocyte polarization effects on fusion events were assayed with IFN- γ (1 ng/ 10^6 cells) and IL-4 (40 ng/ 10^6 cells) 48 h prior to facing CSCs (d_{-2}) to achieve, respectively, M1 and M2 phenotypes.

We next assessed CD36 on H460^{GFP}-CSCs at 50 $\mu\text{g}/\text{mL}$ native LDL (ThermoFisher-L3486), in parallel with previously studied oxLDL, and anti-oxidative conditions (Tocopherol, 50 mM, SIGMA-T3251), by using both H460^{GFP}-CSCwt and H460^{GFP}-CSC silenced with siRNA-CD36. BODIPY oxidation and CD64 (BD555 527) M1-polarization, expressions were recorded.

Exosomes isolation and assessment

H460^{GFP}-CSCs were grown as described (the formulation does not include FBS, and all components are exosomes-free). Monocytes (8×10^6) from buffy-coats were cultured for 6 days with RPMI+10% exosomes-free FBS (Gibco-A25904DG). Supernatants were collected and exosomes vesicles (EVs) were isolated using a standardized protocol.²⁹

To determine EVs size, nanoparticle tracking analysis was performed using a NanoSIGHT LM10 (Malvern, USA) device. For western blot analysis, EVs were broken using a solution of equal parts of protease inhibitors (Complete protease inhibitor cocktail, SIGMA-P8340) and RIPA buffer (ThermoFisher-89900). Monoclonal antibodies α -CD63 (ab134045), α -ALIX (ab117600) and α - β ACTIN (housekeeping, SIGMA-A5316) expression were assessed.

Next, 2×10^3 H460^{GFP}-CSC cells were incubated with 5, 10 or 20 μg of monocytes-exosomes, and 1.8×10^4 monocytes (from HVs) were incubated with 5 or 10 μg of H460^{GFP}-exosomes, in RPMI+10% exosomes-free FBS. A co-culture of 2×10^3 H460^{GFP}-CSC and 1.8×10^4 monocytes (cRPMI) was run in parallel as control. Hybrids (CD14⁺PANK⁺ for monocyte-wells and CD14⁺GFP⁺ for tumors-wells) were analyzed by FACS after 5 days; note that although PANK and GFP expression will be driven by tumor cells, putative hybrid formation after monocytes incubation with H460^{GFP}-exosomes, could only be detected with essential proteins such as PANK.

Statistical analysis

For all the experiments, an adequate sample size was determined using the results of pilot studies and no statistical method was used to determine sample size. Appropriately, t-Student, ANOVA followed by Tukey analysis or Mann-Whitney U tests were performed. The Chi-square was used to evaluate the concordance between PT (primary tumors) and M (metastasis) samples and the association between CD36 and CD36/CD14/PANK with metastasis. To predict metastasis, a logistic regression model was fit with **Cohort#1**, using

circulating THCs (%) and gender (female = 0, male = 1) values as explanatory variables. The resulting formula was used to derive a simple scoring system: we used the weighted sum of the predictors from the logistic regression model multiplied by their regression coefficients, and then transformed these onto the (0.1) interval to yield a predicted probability of metastasis for each patient. Finally, in a validation **Cohort#2**, we estimated the probability of metastasis based on the formula, by examining the area under the curve (AUC) of the Receiver-Operating Characteristic (ROC). Thus, AUC measures how well the model discriminates between metastatic and non-metastatic patients. We also indicated sensitivity, specificity and the 95% Confidence Intervals (95% CI). Significance was set (* $P < .05$, ** $P < .01$, *** $P < .001$, **** $P < .0001$) using Prism 6.0 software (GraphPad) and SPSS software (IBM Corp. Released 2015. IBM SPSS Statistics for Windows, Version 23.0. Armonk, NY: IBM Corp).

Results

Generation of hybrids from *in vitro* fusions between monocytes and tumor stem cells

To test the potential implication of fusion events between monocytes and CSCs in metastasis, human lung cancer cell lines H460^{GFP}, H460 and A549 were cultured in CSC-media under non-adherent conditions to drive tumor-initiating characteristics, including the formation of spheroid aggregates (Supplemental Figure 1a) and expression of proper markers³⁰ (Supplemental Figure 1b and 1c). On the other hand, monocytes were isolated from buffy coats, and fusion assays were performed as shown in Figure 1a, rendering double-positive cells GFP⁺CD14⁺ or PANK⁺CD14⁺, after a strict doublets discrimination (Figure 1b and Supplemental Figure 1d). When co-culturing monocytes stained with vital colorant DID and H460-CSCs with DIO, double-positive cells defined as DID⁺DIO⁺ were quickly detected in about 30 minutes by confocal microscopy (Figure 1c). As these time-lapses were longer quantitatively performed (Supplemental video 1), the population's dynamics showed flat-curve for (non-dividing)-monocytes, exponential-curve for (dividing)-tumor cells, and (≈ 16 h)-lag-period followed by an infinite growth for (emerging)-hybrids (Supplemental Figure 2). We detected significant differences in the efficiency of hybrids generation between CSCs and non-CSCs (Figure 1d). The phenomenon was specific for monocytes, given that lymphocytes and neutrophils co-cultures did not result in hybrids (Figure 1e). Moreover, no significant differences were observed neither among monocytes and macrophages nor in monocytes to macrophages transition in fusion efficiency, as evaluated by specific markers CD14, CD15 and CD36³¹ (Figure 1e and Supplemental Figure 3a-e). Note that CD14/CD15/CD36 levels on monocytes and neutrophils, and CD16/CD16b/CD66b on neutrophils, were analyzed during fusion kinetics monitoring, and fluctuations involving fusion event were related only to the former, since neutrophils die within the first 24 h of culture and do not support any significant proportion to whole fused-population (Supplemental Figure 3f-j). Moreover, CD15, the best marker

describing neutrophils development, should be discarded as it is also expressed by most cancer stem-cell lines,³² including those in this study (Supplemental Figure 3g). Eventually, a similar rate of hybrids was obtained for monocytes and macrophages (Figure 1f).

Of note, no changes in fusion rate were observed neither when monocytes were cultured in the presence of H460^{GFP}-exosomes nor vice-versa (Supplemental Figure 4). Along these lines, Gast *et al.* have described double-positive cells using tumor and myeloid cells of murine origin, and neither detected phenomenon changes when each of them was cultured in the presence of supernatants from the other.¹²

Tumor-hybrid cells show a well-defined identity

As shown in Figure 2a, multi-nucleated DAPI-labeled H460^{GFP}-CSCs co-cultured with EdU-nuclei labeled monocytes generated multi-nucleated hybrids cells with fused-nuclei. This finding mirrors both karyotype and electron-microscopy analyses of hybrids (Figure 2b,c). Although fused-cells preserved tumor-like multiple chromosomal aberrations, they showed a normal number of chromosomes according to diploid cells. They also lost the trisomy at chromosome-16 and an aberrant chromosome-A observed in H460 (Figure 2b) thence a key point to discriminate between fusion and phagocytosis. Moreover, electron-microscopy confirmed the fusion process, showing clearly morphological H460-different,³³ GFP⁺CD14⁺-cells of $10.15 \pm 3.05 \mu\text{m}$, with pseudopod extensions and lamellipodia, large numbers of mitochondria, lysosomes and autophagic vacuoles, and often prominent nuclei surrounded by micronuclei-containing vacuoles (Figure 2c(i-vi)). Remarkably, electron-microscopy also ruled out possible phagocytic events mimicking fusion in cytometry analyses. Furthermore, we investigated transcriptome signatures and pathways characteristic of hybrids by performing RNA-Seq analysis of naïve CD14⁺-monocytes (CD14⁺_n, blue) and cells resulting from fusion protocol (CD14⁺, red; CD14⁺GFP⁺, tangerine and GFP⁺, green). A principal component analysis (PCA) positioned hybrids far from CD14⁺_n and in-between CD14⁺ and GFP⁺ cells (Figure 2d). At the molecular level, this result can be explained by the co-occurrence of transcriptional signatures of both cell types in hybrids (Figure 2e,f). A thorough analysis of RNA-Seq data revealed that, transcripts associated with cancer and expressed primarily in GFP⁺, as well as transcripts involved in immune-associated pathways and expressed primarily in CD14⁺, were expressed by hybrids (Supplemental Figure 5a and 5b). A number of these genes were validated by RT-qPCR (Supplemental Figure 5c). Note also that CD14⁺ and CD14⁺_n cells are quite different at the transcriptomic level (Supplemental Figure 6); the former shows a contrasting activated phenotype due to their interactions with the CSCs.³⁴

Ultimately, FACS analysis showed that, according to both RNA-Seq and CSCs phenotypes (Supplemental Figure 1c and Supplemental Figure 5), hybrids were mainly CD14⁺-cells expressing cancer-epithelial-cytokeratins markers (PANK) and CD36 (i.e., a CD36⁺CD14⁺PANK⁺ signature, Figure 2g); hence, we coined as Tumor-Hybrid Cells (THC).

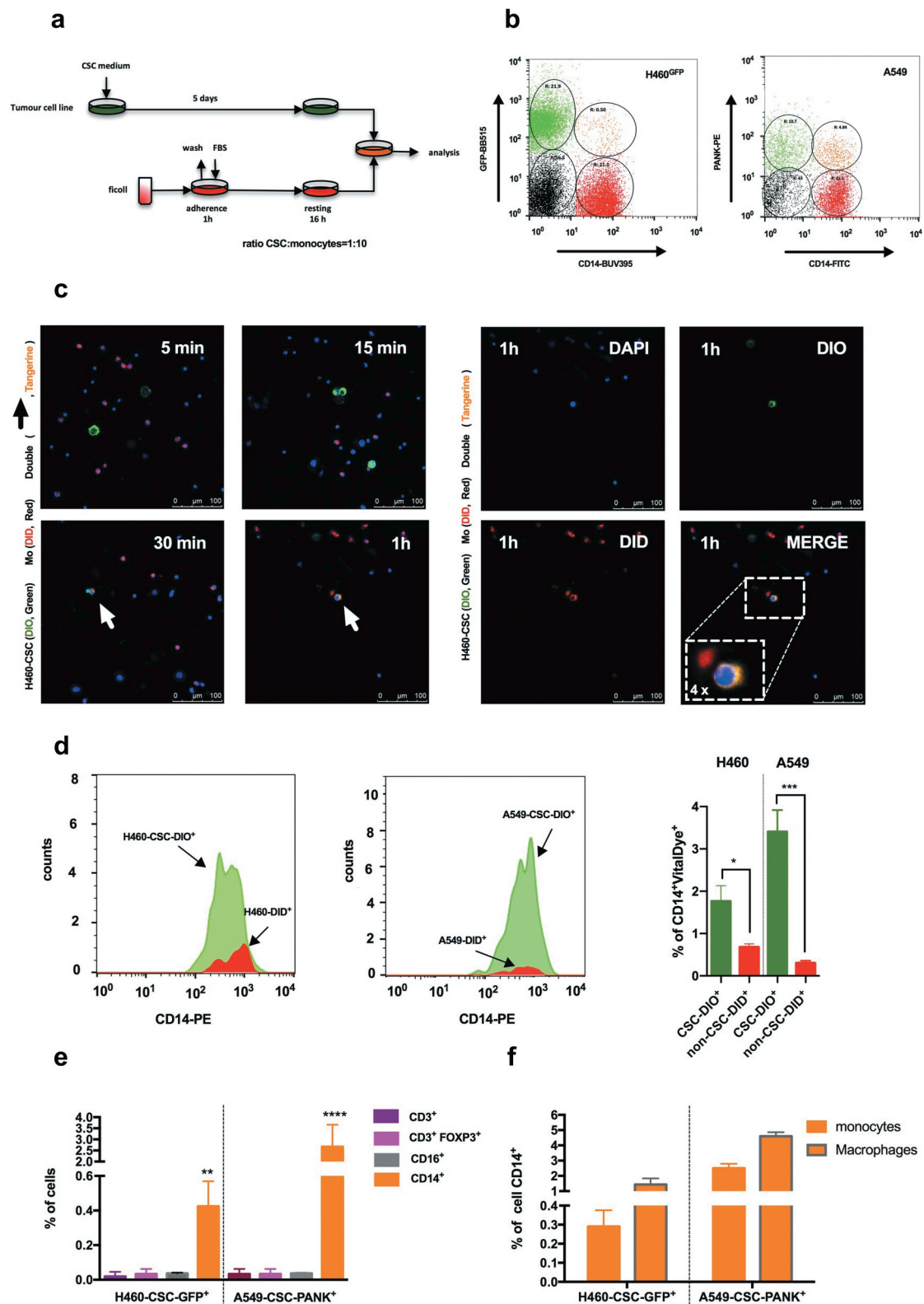


Figure 1. Co-culture *in vitro* of cancer stem cells and human monocytes generates hybrid cells. (a) Pipeline for *in vitro* fusion assays between cancer stem cells (green) and PBMCs' isolated monocytes (red, CD14⁺). (b) Representative FACS analysis ($n = 9$; GFP⁺ and PANK⁺, green; CD14⁺, red) of hybrids yielding after 5 days of fusion assays with H460^{GFP}-CSC (tangerine in left panel, GFP⁺CD14⁺) and A549-CSC (tangerine in right panel, PANK⁺CD14⁺). (c) Representative confocal images of double-positive events with vital colorants DIO (green, H460-CSC), DID (red, monocytes) and DAPI for nuclei (blue), after 5 min (i), 15 min (ii), 30 min (iii) and 1 h (iv) of co-culture (left panel); arrows indicate double-positive events (co-localization, tangerine), $n = 3$. In the right panel, the representative image at 1 h (iv) in the left panel, is first unmerged for the three channels (v, blue; vi, green; vii, red) and then magnified (4x) to clearly showing merged (viii) colors in a hybrid cell. (d) Representative overlay of histograms for FACS analysis of resulting fusions between human monocytes and H460-CSC (green, DIO⁺) vs. H460 (red, DID⁺) in the left panel, and A549-CSC (green, DIO⁺) vs. A549 (red, DID⁺) in the central panel, in a competition assay in which equal quantities of DIO⁺ and DID⁺ tumor cells were co-cultured with CD14⁺ monocytes for 5 days (ratio tumor cells:monocytes = 1:10). In the right panel, statistical resume of the results ($n = 3$; * $p < .05$, *** $p < .001$, two-tailed t -test, data are mean \pm SD). (e) Analysis of resulting fusion events between H460^{GFP}-CSC (left) and A549-CSC (right) with lymphocytes (CD3⁺), Treg (CD25⁺ FOXP3⁺), neutrophils (CD16⁺) and monocytes (CD14⁺) (for each one, $n = 3$; ** $p < .01$, **** $p < .0001$, two-tailed t -test, data are mean \pm SD). (f) Analysis of hybrids yielding from fusions between H460^{GFP}-CSC (left) and A549-CSC (right) with monocytes or macrophages (bordered bars) after 5 days of co-cultures.

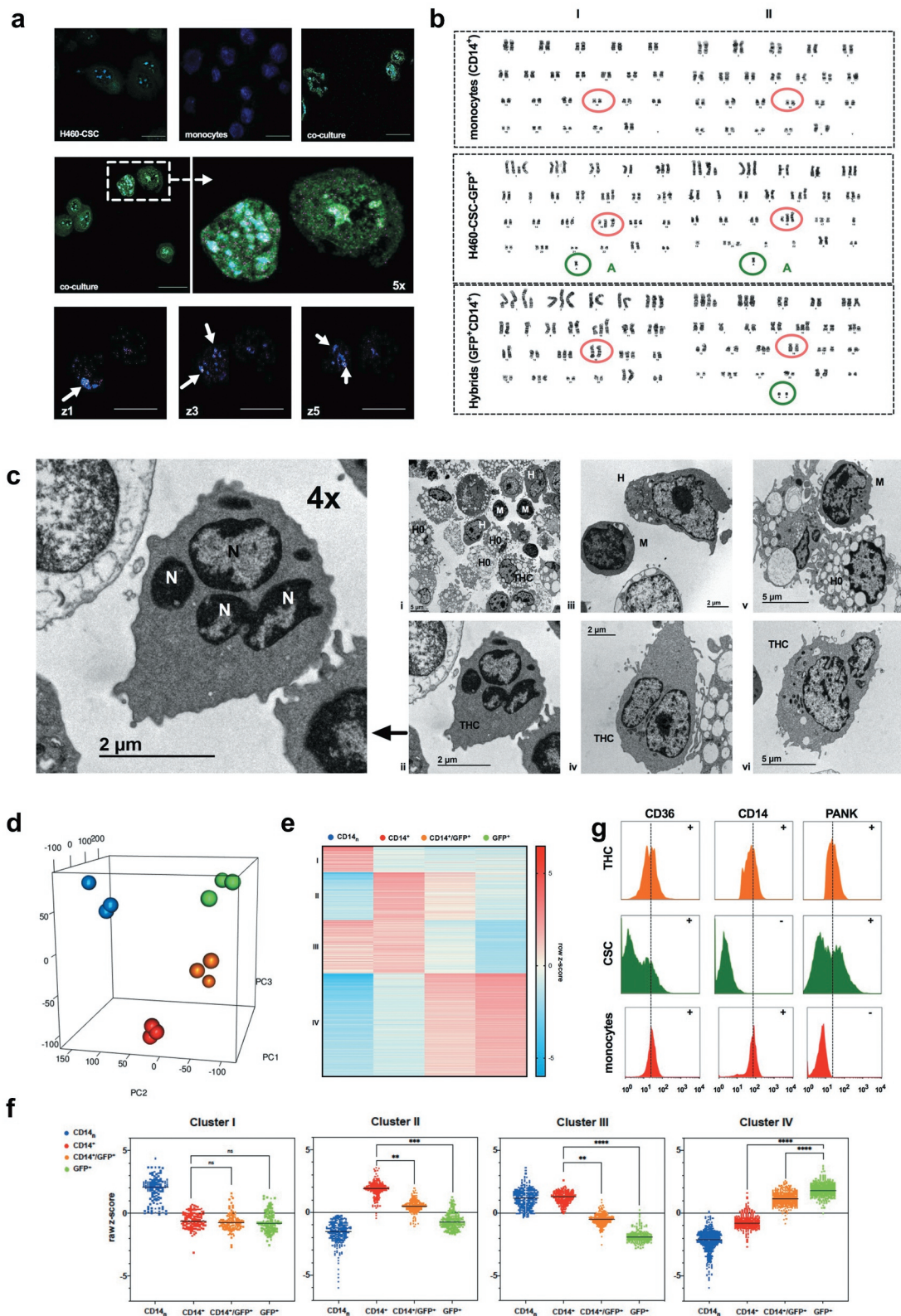


Figure 2. Fused-cells exhibit a patent entity. (a) Representative confocal images of co-cultures between DAPI-labeled H460^{GFP}-CSC and EdU-labeled monocytes (630x magnification, scale 25 μm): DAPI (blue), EdU plus secondary Alexa-647 (purple), GFP (green). First row: (left) lone control H460^{GFP}-CSCs showing green cytoplasm and blue nuclei; (central) lone control monocytes showing purple nuclei; (right) panoramic view of the co-culture. Second row: (left) a co-culture highlighting a fused cell close to a tumor cell; (right) 5x zoom of previous framed cells showing blue/purple fused nuclei, with a green cytoplasm. Third row: three other z-axis planes (z1, z3 and z5, scale 20 μm) of previous picture highlighting (white arrows) fused nuclei. (b) After fusion, cells were sorted and the karyotype of the different fractions checked (CD14⁺, GFP⁺ and GFP⁺CD14⁺). Differences are marked, salmon circle: losing the trisomy after fusion at the 16 chromosome, clover circle: extra aberrant chromosome A that is lost or starts to disappear after fusion. (c) Representative electron-microscopy photographs: (i) panoramic view of the co-culture, highlighting monocytes (m), dying tumor cells (H0), live tumor cells (h) and hybrids (THC); (ii) a fused cell showing dense cytoplasm with heterochromatic nuclei (n), and then magnified (4x) at its left side; (iii) a monocyte close to a live tumor cell; (iv) hybrid with prominent nuclei, pseudopod extensions and lamellipodia; (v) a monocyte close to a dying tumor cell with

CD36 on lung primary tumor is crucial for the generation of THCs

Expression of CD36 by CD14⁺PANK⁺ hybrids seemed relevant as this scavenger-receptor not only had been recently reported to play a key role in the context of metastasis,^{35,36} but also because of its known fusogenic activity.³⁷ Moreover, as we moved to evaluate CD36 in H460, we noticed its expression increases either as mRNA (Figure 3a) or protein (Figure 3a insert) only in CSC-media, as H460 acquired stemness (Supplemental Figure 1). Therefore, we passed to assess the role of CD36 expression in mediating fusion amongst myeloid and tumor cells. The up-regulation of CD36 in both CSCs and monocytes (Figure 3b) by hydroxyalkenal activator (4HNE)³⁸ resulted in a significant increase of THCs (Figure 3c). CD36 was then separately over-expressed in monocytes and H460^{GFP}-CSC (Figure 3d). Only for H460^{GFP}-CSC transfected with pCD36, an increase in THC events was observed (Figure 3e). However, no significant increment was found when monocytes overexpressed CD36 by even two different protocols (Figure 3f and insert). Consistently, though RNA-silencing reduced CD36 expression on both H460^{GFP}-CSCs and CD14⁺-cells (Figure 3g), a significant reduction of hybrid occurrence was only observed for the former (Figure 3h); CD36 downregulation on CD14⁺-cells did not affect fusion rate as much as the presence of α -CD36 (Figure 3h). Remarkably, clone A549-B10, a CRISPR-engineered p.(Glu46Argfs*7) A549-CD36 $\Delta\Delta$ cells (Figure 3i and Supplemental Figure 7), which consequently did not yield THCs if co-cultured with monocytes, was able to rescue normal fusion values after transient-transfection with pCD36 (Figure 3j).

Taking into account CD36 affinity for oxidized molecules,^{38–40} we modified monocytes oxidative state by intermediate-metabolism manipulation^{41,42} (Figure 3k), finding that their oxidative boost after oxidizing low-density lipoprotein (oxLDL) treatment also provoked their polarization to M2-phenotype⁴³ (Figure 3l). Likewise, the presence of lactate during the last 16 h of fusion-lag induced the same effect on monocytes,^{41–44} in contrast to longer lactate incubation periods (96 h), which in turn reverted to M1-phenotype (Figure 3l). Altogether, the oxidative boost and M2-polarization matched the increment in THCs (Figure 3m); note that those CD14⁺ cells that did not fuse in previous experiments showed an M1-polarization genotype (Supplemental Figure 6). It is noteworthy that previous IL4-polarization to M2-monocytes increased the hybrids formation ratio (Figure 3n). We observed that the oxidative state was also higher for IL4-treated monocytes than both control and IFN γ -treated cells (Figure 3o). Other authors have previously reported that M2-phenotype favored fusion events.⁴⁵ As expected, these phenomena were closely dependent on microenvironmental oxidative status, since native LDL was unable to boost neither oxidized (Figure 3p) nor M2-monocytes (Figure 3q). Moreover, CD36-silencing for oxidative and non-oxidative microenvironmental

conditions, and in the presence of tocopherol (a potent antioxidant and inhibitor of CD36⁴⁶) confirmed this scavenger-receptor to be crucial for the fusion event (Figure 3r).

THCs show a high rate of migration and proliferation

To explore whether fusion conferred any advantage to THCs in terms of migration and invasiveness, we performed both collagen-free and collagen (membrane) migration assays (Figure 4a, insert panel). The percentage of migrated cells showed clear differences between THCs and CSCs in passive (no membrane) and active migration. GFP⁺CD14⁺ but not H460^{GFP}-CSCs, reached the lower compartment while, as expected, most human monocytes migrated through the insert (Figure 4a, left panel). Similar findings were obtained with THCs (PANK⁺CD14⁺) generated from A549 (Figure 4a, right panel).

To test hybrids proliferative ability, CFSE assays were performed and higher proliferation rates of THCs than H460^{GFP}-CSCs (Figure 4b) were found. Moreover, after 20 days of sole single-cell seeding, a proliferative activity was documented (Figure 4c). Interestingly, those *in vitro* generated tumors were quite heterogeneous for a set of tumoral markers (PD-L1, EpCAM and cytokeratins), which might be a clue to explain metastases heterogeneity, though further *in vivo* studies will be needed (Figure 4c, insert).

Migration ability was also observed *in vivo*. When inoculating mice with THCs or H460^{GFP}-CSC, a distribution pattern consistent with previous reports,⁴⁷ after evaluations at 3, 6 and 28 weeks post injection, was shown (Figure 4d). Most injected cells reached the lungs after 3 weeks. However, after 6- and 28-weeks THCs but not CSCs were found in lungs and lymph nodes, suggesting that THCs were able to colonize and then migrate to distant sites. In addition, when we came across spleens, a well-known tissue where metastasis by primary lung cancer organotropism cannot be justified by circulatory pattern,⁷ we found that those mice inoculated with THCs had developed unstructured spleen morphology, with no demarcated limits among white and red pulps and THC-lumps development with tumor appearance (Supplemental Figure 8); high levels of TTF-1 lung cancer-marker expression were detected, emphasizing the lung-metastatic features (Supplemental Figure 8). Moreover, orthotopic *in vivo* model of metastasis showed that CD45⁺/Cytokeratin-8⁺ cells were present in the peripheral blood of mice bearing tumor development after 5 weeks (Supplemental Figure 9). As a whole, these data concur with previously reported in mice models showing metastasis-related fusion events in mice models.¹²

THCs avoid immune control

Following the experimental design shown in Figure 5a, we moved to study the immune response against hybrids. As

autophagic vacuoles; (vi) a bi-nuclei hybrid with large numbers of small electron-dense mitochondria, lysosomes, surrounded subcellular organelles and abundant rough endoplasmic reticulum. (d) PCA of row Z-scores showing separation of the four cell populations (naïve CD14⁺, blue; and the resulting cell populations after fusion protocol and sorter: CD14⁺, red; CD14⁺GFP⁺, tangerine; GFP⁺, green) (e) Z-score heat-map showing the major gene clusters (I–IV) (f) Differences among the four cell types for clusters (I–IV), mean, **p < .01, ****p < .0001 one-way ANOVA. (g) Protein expression (FACS) of key surface markers to track the cellular components of the fusions: THCs (CD36⁺CD14⁺PANK⁺, tangerine), CSC (CD36⁺CD14⁺PANK⁺, green) and monocytes (CD36⁺CD14⁺PANK⁻, red), representative histograms (n = 3).

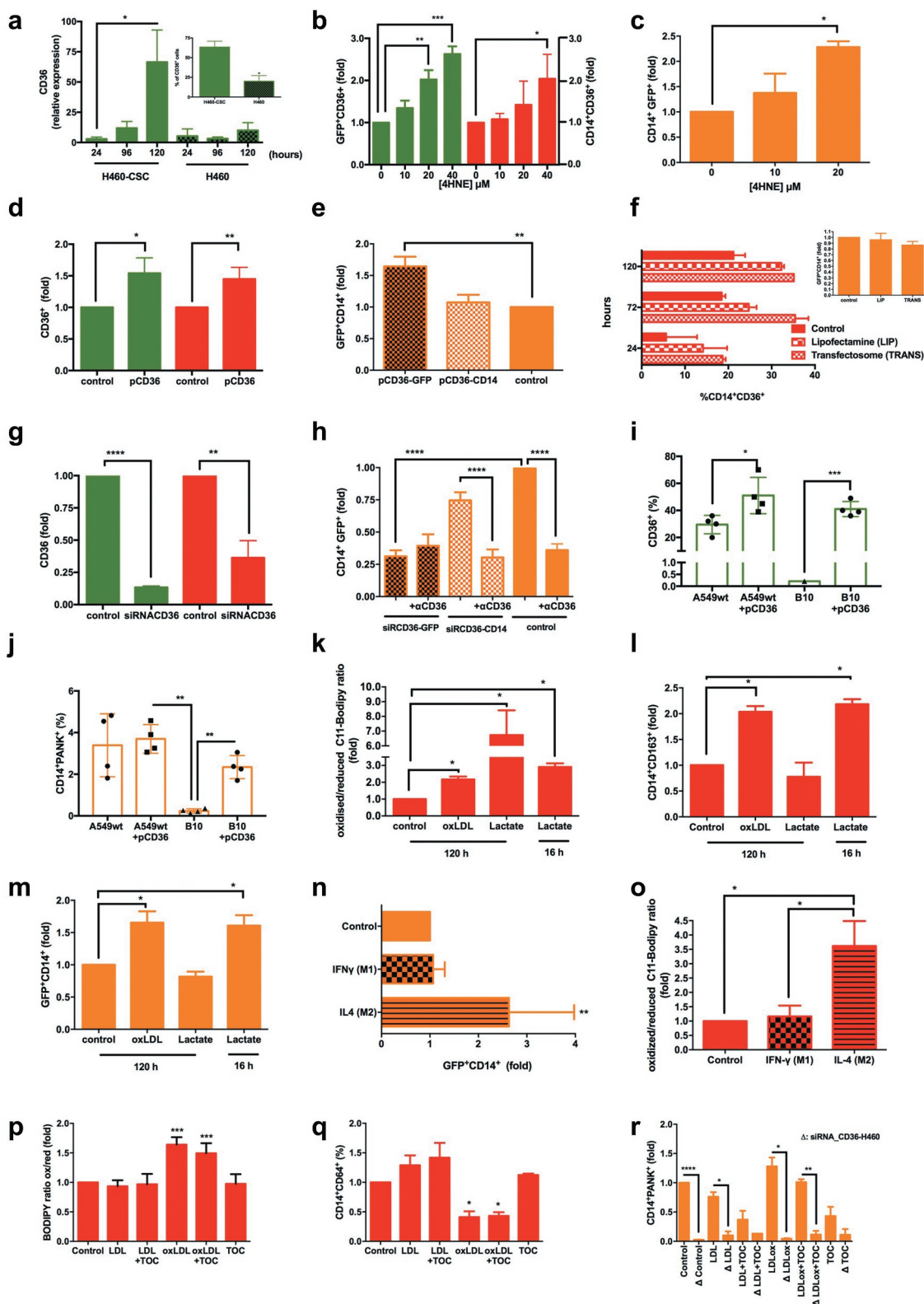


Figure 3. Fusion process efficacy depends on both the regulation of CD36 expression by CSCs and microenvironmental lipids fluctuations, and the oxidative status and M2-phenotype of MΦs. (a) Relative CD36 mRNA (RT-qPCR) expression of conditioned stem-like H460-CSC vs. native H460 cells, followed-up for 5 days ($n = 7$, $*p = .003$, one-way ANOVA/Tukey's); Insert, FACS percentage of CD36⁺ cells at the end of the assay ($n = 7$, $*p < .05$, two-tailed t-test). (b) Overexpression (FACS) of CD36 in both CSCs (green) and monocytes (red) by 4HNE ($n = 3$, $*p < .05$, $**p < .01$, $***p < .001$, two-tailed t-test). (c) Resulting fusion rates after 4HNE incubation; 40 μM was lethal ($n = 3$, $*p = .004$, one-way ANOVA/Tukey's). (d) Specific pCD36 overexpression on CSCs (green) or monocytes (red) ($n = 3$, $*p = .018$, $**p = .014$, two-tailed t-test). (e) Resulting fusion rates with CD36 overexpressing CSCs (brown) or monocytes (light orange) vs. a control co-culture (orange) ($n = 3$, $**p = .005$, one-way ANOVA/Tukey's). (f) Two other ways to overexpress CD36 on monocytes ($n = 2$) and resulting fusion rates with CSCs ($n = 2$, insert). (g) Specific downregulation of CD36 on CSC (green) or monocytes (red) using siRNA-CD36 ($n = 3$, $**p = .0012$, $***p = .0001$, two-tailed t-test). (h) Effects of siRNA-CD36 combined with α -CD36 and resulting fusion rates ($n = 6$, $****p < .0001$, two-tailed t-test). (i, j) CD36 CRISPR-engineered KO abolish fusion event. (i) Increased levels of CD36 protein expression (FACS) by wild type A549-CSCs and clone B10, a CRISPR-engineered A549-CD36 Δ/Δ -CSC clonal line, after transfection with pCD36 48 h before starting co-cultures with monocytes ($n = 4$, $**p < .05$, $***p < .001$, two-tailed t-test). (j) Fusion event is rescued after B10 clone starts overexpressing CD36 ($n = 4$, $**p < .01$, two-tailed t-test). (k) Effects of stimulation with

THCs were exposed to expanded human NK-cells, significant downregulation of immune response was observed: perforin generation by CD3⁻CD56⁺CD16⁺ cells was reduced⁴⁸ (Figure 5b) and cytotoxicity significantly decreased (Figure 5c). Note that, hybrids exhibited a higher expression of well-known NK-cells inhibitors HLA class I members (HLA-B and HLA-E) than CSCs (Supplemental Figure 5). However, though the expression of TGF- β was higher in hybrids than CSCs and monocytes (Figure 5d), it was not significant enough to explain the effect observed in NK-cells.⁴⁹ Interestingly, both CD4⁺ and CD8⁺ T-cells showed a marked reduction in mitogen-induced proliferation after exposition to THCs with regards to CSCs (Figure 5e,f). This effect was reverted in the presence of either α -PD-1 or a cocktail of α -CD39, α -CD73 and α -SIGLEC5 (Figure 5g,h). According to our RNA-Seq analysis, these four molecules exhibited higher expression in hybrids than CSCs (Supplemental Figure 5), a pattern that was also verified by FACS (Figure 5i).

In agreement, a differential pro-inflammatory cytokine production was observed when hybrids and CSCs were co-cultured with PBMCs from HVs (Supplemental Figures 10a and 10b). Whilst CSCs up-regulated IFN γ , TNF α and IL-6, THCs did not. A global analysis of FoxP3 expression (master regulator of T_{reg} cells) by PBMCs, and the immune checkpoints PD-1 and CTLA4, indicated an up-regulation of these regulatory factors when PBMCs interact with THCs (Supplemental Figure 10c, upper panel) with regards to CSCs (Supplemental Figure 10c, lower panel). Besides, overexpression of FoxP3 and PD-1 on CD4⁺-lymphocytes, and PD-1 and CTLA4 on CD8⁺-cells were induced by THCs but not by CSCs, as seen after co-culturing them with PBMCs (Supplemental Figure 10d). It is also noteworthy the differences observed in T_{reg} and CD8⁺ T cells proliferation, after blocking the fusion essential-receptor CD36 in co-cultures of HVs' lymphocytes with either CSCs or THCs. According to a mechanism recently reported,⁵⁰ CD36-blockade T_{reg} cells were not able to expand in a CSCs' microenvironment (Supplemental Figure 11a) then allowing anti-tumoral CD8⁺ T cells to proliferate (Supplemental Figure 11b). However, this effect seemed attenuated in THCs' microenvironment. Whether or not a metabolic modulation involving CD36 amongst T_{reg} cells and THCs occurs, will need further *in vivo* studies. Altogether, these data evidence THCs are able to both modulate and overcome immune surveillance.

THC-specific markers signature on primary lung tumors and in circulation correlate with metastatic events

We next used the signature CD36/CD14/PANK to localize "Trojan horses" in tissues and peripheral blood of lung cancer patients, looking for a correlation between dissemination pattern and origin of these metastatic cells. Notably, analysis of CD36 alone and the triad, along 87 lung samples from normal

tissue (healthy, n = 4), inflammatory tissue (chronic pneumonia, n = 8) and lung cancer (squamous cell carcinoma, n = 29; adenocarcinoma, n = 3; adenocarcinoma, n = 28; small-cell carcinoma, n = 9; bronchioloalveolar carcinoma, n = 1; large-cell undifferentiated carcinoma, n = 1; and papillary adenocarcinoma, n = 4) revealed high levels of CD36 in a number of these samples. However, there was no correlation with metastasis occurrence (Chi-square = 2.093, *P* = .148, Person Test) (CD36 columns in Figure 6a, Supplemental Figure 12, left panel and Supplemental Table 2). In contrast, triple-positive-cells were found only in the lungs of those patients who subsequently suffered metastasis (CD36/CD14/PANK columns in Figure 6a, left panel in Figure 6b, CD36/CD14/PANK column in Supplemental Figure 12, and Supplemental Table 2). There was a significant correlation between CD36/CD14/PANK co-localization in lung samples and metastasis occurrence (Chi-square = 36.737, *P* < .001, Pearson test, Supplemental Table 2).

Remarkably, CD36⁺CD14⁺PANK⁺ cells were found in 60% of the primary tumors of those patients who subsequently developed metastasis (40 out of 87 patients) and the signature was also found in 80% of the metastatic tissues (Figure 6b, Supplemental Figure 12 and Supplemental Table 2). Besides, paired samples (primary tumors and their corresponding metastases) were not significantly different in this regard (n = 40, Chi-square = 0.395, *P* = .530, Supplemental Table 2).

On the other hand, following strategy shown in Supplemental Figure 13, presence of THCs was evaluated in circulating cells from 50 patients diagnosed with pulmonary tumors (Cohort#1, I in Supplemental Table 3) often metastatic, 24 HVs and 20 septic patients without any clinical history of cancer-related pathologies were also analyzed as controls (Figure 6c). THCs were not found in controls. However, lung cancer patients were positive for CD36/CD14/PANK signature. These patients had been diagnosed at a late stage and were included in the study before chemotherapy. In agreement, the presence of THCs correlated to the size and direct extent of the primary tumor as defined by the TNM (Spearman's Rho = 0.447; *P* = .006). Moreover, when patients were classified into two groups according to the median of THC (%) in circulation (Figure 6c and Supplemental Figure 14), those patients above the median showed significant correlation with size of the primary tumor (T, Spearman's Rho = 0.797; *P* < .001), spread to regional lymph nodes (N, Spearman's Rho = 0.723; *P* = .001) and stage (Spearman's Rho = 0.447; *P* = .025). These results were further used to predict the metastatic status of another cohort of 28 patients with lung cancer (Cohort#2, II in Supplemental Table 3), showing that together %THC and gender may predict metastasis in a high extent (Supplemental Figure 15; AUC = 0.821; 95%CI, 0.679 to 0.963; *P* < .0001).

oxLDL or lactate (at two time-points of fusion: the last 16 h or a total of 96 h) on monocyte oxidative status (n = 4, **p* = .02, one-way ANOVA/Tukey's). (l) CD163 M2-polarization measure of previous monocytes (n = 4, **p* = .01, one-way ANOVA/Tukey's) (m) Resulting fusion rates with previous monocytes (n = 4, **p* = .03, one-way ANOVA/Tukey's). (n) Fusion rates reached under canonical (M1) vs. noncanonical (M2) stimulation of monocytes by either IFN- γ or IL-4, respectively (n = 3, *****p* = .006, one-way ANOVA/Tukey's). (o) Oxidative status of monocytes on both previous conditions (n = 3, **p* = .017, one-way ANOVA/Tukey's). (p, q) Effects of stimulation with LDL or oxLDL, alone or supplemented with tocopherol, as well as the latter alone on monocytes. (p) Oxidative status (n = 3, ****p* < .001, two-tailed t-test) and (q) CD64 expression for M2-polarization measurement on CD14⁺ cells (n = 3, **p* < .05, two-tailed t-test). (r) Effects of downregulate CD36 (siRNA-CD36) on H460-CSCs prior to co-culture with monocytes, then stimulating with LDL or oxLDL, alone or supplemented with tocopherol, as well as the latter alone, on hybrids yielding (n = 3, **p* < .05, ***p* < .01, ****p* < .0001, one-way ANOVA/Tukey's). Data in A-R are mean \pm SD.

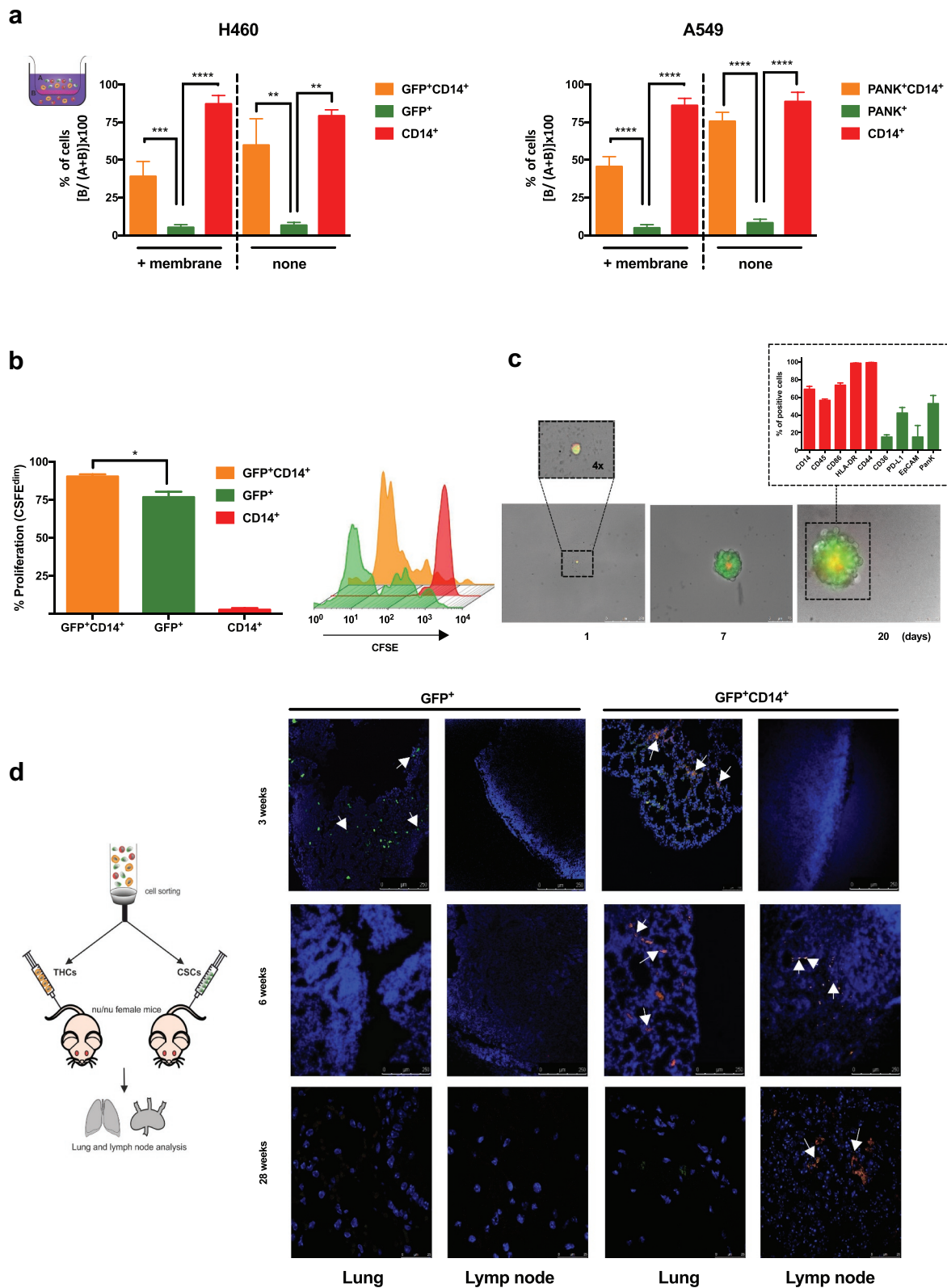


Figure 4. THCs show migration and proliferation capabilities both *in vitro* and *in vivo*. (a) Active and passive migration of the various populations involved in the fusion process. Left insert, a diagram of transwells showing the non-migrated cells (A) in the top chamber, and migrating cells (b) in the bottom chamber. Results for migration of fusion assays components from H460^{GFP}-CSC (center) and A549-CSC (right) co-cultures, performed with (left side of each graph) or without a collagen-covered membrane (right side of each graph). Hybrids (GFP⁺CD14⁺ or PANK⁺CD14⁺, for H460^{GFP} or A549, respectively), orange bars; CSCs (idem, GFP⁺ or PANK⁺), green bars; monocytes, red bars (n = 3, **p < .01, ***p < .001, ****p < .0001, one-way ANOVA/Tukey's, data are mean ± SD). (B) Proliferation rate differences amongst the three sorted cell types as measured by CFSE dimming after 7 days of growth (n = 3, *p = .01, one-way ANOVA/Tukey's, data are mean ± SD); and a representative diagram of proliferative cells (insert). (c) After 5 days, co-cultures of H460^{GFP}-CSC and monocytes were sorted and single hybrids seeded on 96-well plates, then followed-up during 20 days (a representative experiment is shown, a 1-day single cell is shown 4x magnified; n = 45); Insert, 20 days old tumors expression of several markers (n = 5, data are mean ± SD). (d) Mice experimental design (left) for *in vivo* hybrid invasiveness characterization. Lungs and lymph nodes (right) were analyzed for the presence of GFP⁺ (H460^{GFP}-CSC) and GFP⁺CD14⁺ (hybrids) cells after 3, 6 and 28 weeks (n = 5 for each treatment) of i.v. tail inoculation.

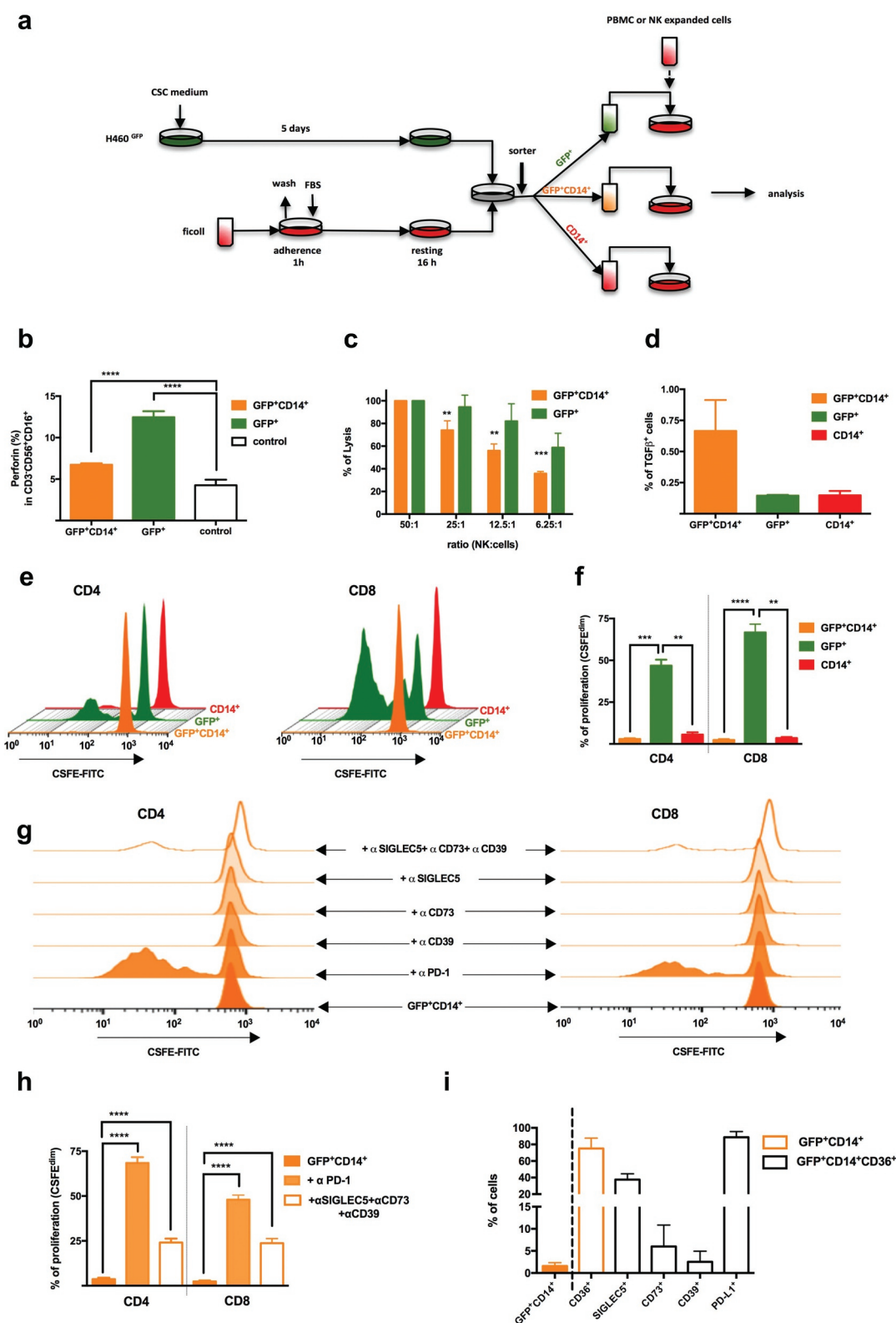


Figure 5. THCs downregulate *in vitro* immune response. (a) Pipeline of the procedure to study the immune response. Tumor cells (green) were grown to CSC and co-cultured with monocytes (red); then, H460^{GFP}-CSCs (green, GFP⁺), hybrids (orange, GFP⁺CD14⁺) and monocytes (red, CD14⁺) were sorted and independently seeded with either PBMCs or NK cells from HVs. (b, c) Immunogenicity of sorted hybrids vs. H460^{GFP}-CSC, exposed to expanded human NKs, as measured by: (b) perforin generation by CD3⁺CD56⁺CD16⁺ cells (n = 4, ****p < .0001, one-way ANOVA/Tukey's, data are mean ± SD) and (c) lysis at various NK cells:cell ratios (n = 3, **p < .01, ***p < .001, two-tailed t-test, data are mean ± SD). (d) Protein expression (FACS) of intracellular TGFβ in hybrids (orange), H460^{GFP}-CSCs (green, GFP⁺) and monocytes (red, CD14⁺); n = 5. (e, f) CFSE-labeled PBMCs from HVs were exposed (ratio 1:5) to sorted hybrids (orange, GFP⁺CD14⁺), H460^{GFP}-CSC (green, GFP⁺) and monocytes (red, CD14⁺): (e) representative graphs for mitogen-induced proliferations, defined as CFSE^{dim}, of both CD4⁺ (left) and CD8⁺ (right) cells, and (f) statistical resume of the data (n = 4, **p < .01, ***p < .001, ****p < .0001 two-tailed t-test, data are mean ± SD). (g, h) CFSE-labeled PBMCs from HVs were stimulated with pokeweed (PWD) and exposed (ratio 1:5) to lone sorted hybrids (GFP⁺CD14⁺) or added with either αPD-1, αCD39, αCD73, αSIGLEC5, or a cocktail made of the last three ones: (g) representative graphs for proliferations, defined as CFSE^{dim}, of both CD4⁺ (left) and CD8⁺ (right) cells, and (h) statistical resume of the data (n = 4, ****p < .0001, two-tailed t-test, data are mean ± SD). (i) Protein expression of membrane-anchored CD36, SIGLEC5, CD73, CD39 and PD-L1 (empty black bars) in hybrids (empty orange bar, left of the dotted line); n = 5 (data are mean ± SD).

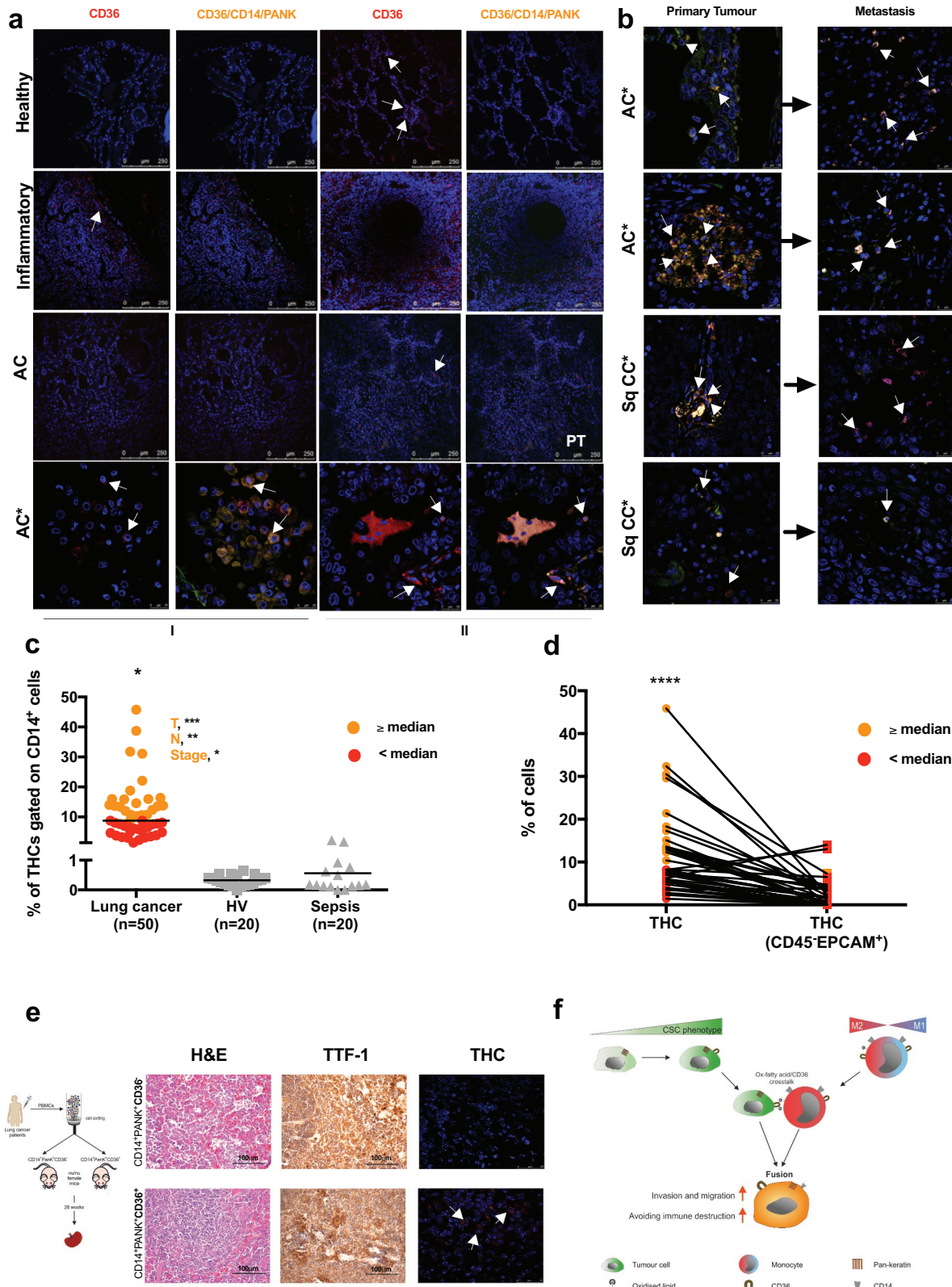


Figure 6. THCs specific markers signatures in patients with lung cancer. (a) Expression of CD36 and co-localization of the signature CD36/CD14/PANK on lung tissue samples from two sets (I and II) of controls, and patients with: non-tumor-related cancer inflammatory disease (inflammatory), adenocarcinoma (AC) and metastatic adenocarcinoma (AC*) (representative cases from n = 87; see Supplemental Table 2). (b) Co-localization of the signature CD36/CD14/PANK on primary tumor and metastasis samples from patients with metastatic adenocarcinoma (AC*) and squamous carcinoma (SqCC*) (representative cases from n = 87, see Supplemental Table 2 and Supplemental Figure 12). (c) Percentage of THCs, PANK⁺CD36⁺ on gated CD14⁺ circulating cells from patients with lung adenocarcinoma (n = 50) vs. healthy volunteers (HV, n = 20) or patients with sepsis (n = 20) (*p < .0001, one-way ANOVA). Two groups are shown according to median (tangerine dots > median, red dots ≤ median), being that above median in significant correlations with primary tumor size (T, ***p < .001), spread to lymph nodes (N, **p = .001) and stage (*p = .025), as ranked by Spearman's coefficient. (d) Percentage of THCs that exhibited the main characteristic of CTCs (CD45⁻EPCAM⁺) (****p < .0001, paired t-test). (e) Mice experimental design (left) for *in vivo* invasiveness characterization of THCs (CD36⁺CD14⁺PANK⁺) vs. non-THCs (CD36⁻CD14⁺PANK⁺) cells isolated from lung cancer patients' PBMCs. Spleens (right) were analyzed for histopathological changes (haematoxylin/eosin, H&E), metastatic thyroid transcription factor-1 (TTF-1) expression and the presence of metastatic THCs (CD36⁺CD14⁺PANK⁺), 28 weeks (n = 3 for each treatment) after inoculation (also see Supplemental Table 4). (f) Schematic diagram of the proposed mechanism for Trojan horse cells (THC)-driven metastatic fusion.

Curiously, THCs ultimately did not exhibit the main markers of CTCs (CD45⁻EPCAM⁺ on THCs gate, Figure 6d, see gating strategy in Supplemental Figure 13), reinforcing their uniqueness. Finally, when CD36⁻CD14⁺PANK⁺ and CD36⁺CD14⁺PANK⁺ subpopulations from lung-cancer patients' PBMCs were inoculated into mice, only the latter was found in spleens after 28 weeks, along with unstructured morphology and high levels of TTF-1 (Figure 6e and Supplemental Table 4).

Discussion

In this study, we have showed that tumors might “exploit” myeloid cells to expand toward other organs, following the rationale of Paget's ‘seed and soil’ theory. THCs are able to free from primary lung-tumors then exhibiting almost all reported hallmarks of both cancer and metastasis,⁵¹ including motility, microenvironment modulation, genome uniqueness, proliferation and active colonization of distant organs – even some not explained by the circulatory pattern-. On the other hand, though several theories have been proposed to formulate the origin of metastatic cells,⁵² only the “cancer cell fusion” theory seems strong enough to explain THCs emergence data, by a mechanism (Figure 6f) involving CD36, a scavenger-receptor also essential in their dissemination with the proper phenotype. Thence, these results grasp an adequate empirical support to linking both origin and dissemination pattern of metastatic cells in the body.

Our data indicate that fusion between macrophages/monocytes (MΦs) and CSCs takes place with a high dependency on CD36 expression by the latter, and polarization and oxidative status of MΦs. CD36 in its scavenger-receptor function adapts tumor cells to the fluctuating microenvironmental conditions mainly related to fuel supply, and through its fusogenic function recruits major M2-oxidized MΦs to complete fusion process for rendering THCs. In agreement with these observations, other authors³⁵ have shown that neutralizing antibodies against CD36 cause inhibition of metastasis in immunocompetent orthotopic mouse models of human oral cancer. Altogether, these features open new horizons to explore CD36 in both cancer origin and metastasis therapeutics.

Due to the important role of the immune system in the elimination of aberrant cells, escaping from immune control is crucial for cancer and metastasis. Along these lines, *in vitro* obtained THCs expressed high levels of the immune checkpoint ligand PD-L1 and reduced CD8⁺-lymphocytes proliferation in a PD-L1/PD-1 interaction-dependent manner. Other molecules such as SIGLEC5, CD73 and CD39 were found overexpressed on THC, albeit only a significant effect on the interaction with T cells was observed when these three immune-modulators were simultaneously blocked. The presence of THCs induced a downregulation of NK-cells activity and an anti-inflammatory profile in T-cells, together with a modulation of T_{reg} cells. Eventually, from *in vivo* approaches, we have learnt that human THCs are able to reach and colonize distant sites, and also to circulate in the peripheral blood of mice orthotopic metastasis models, hence demonstrating their potential to evade the immune surveillance.

Previous clinical reports have already supported the theory of cancer cell fusion to explain the origins of metastatic cells.¹²⁻¹⁶ Our data demonstrate the presence of THCs in patients with lung cancer. The identification of these cells, through CD36/CD14/PANK signature, in lung samples from patients who have had metastatic lung tumors, strongly supports a role for the hybrids in this context. Furthermore, finding the same THCs in their metastases suggests these must travel from the primary site to the final stage. These circulating cells have also been found in patients with cancer with an outcome of metastasis, but neither in healthy donors nor in patients with an unrelated inflammatory pathology. Remarkably, the detection of THCs in primary tumors correlated to metastasis incidence in the analyzed cohorts. In fact, the frequency of patients with CD36/CD14/PANK co-localization in primary tumor and who did not develop metastasis was zero. Similar results were obtained when we analyzed paired samples of primary tumors and metastases from the same patient, and a statistical correlation between the identification of THCs in primary tumors and metastatic samples was observed. Besides, we were able to predict metastasis occurrence in new lung cancer patients based on their circulating THCs and gender. A critical evaluation of these data could indicate that, as well as in primary tumors, THCs in metastases could be a result of new fusions between tumor and myeloid cells in this niche. Based on our data from human samples, we are not able to answer this question properly. However, previous reports have suggested that patients treated with Denosumab, a potent fusion inhibitor, exhibited a significant reduction of metastasis compared with non-treated population,⁵³⁻⁵⁵ hence, even in case of *de novo* THCs presentation, our model might remain valid for new treatments development.

Finally, it is noteworthy that no influence of either CTCs or exosomes could be inferred from our data. Regardless of the controversy that several studies have shown a role for both CTCs and exosomes in the metastasis fusion context^{4,56,57} whilst some others have not,^{12,58,59} our data did not exclude the importance of these two factors. First, we have demonstrated that THCs are independent events from CTCs but we did not dive into properties of the latter since it was not the aim of this study. Secondly, despite our findings had indicated that THC generation is independent of the presence of exosomes derived from their parental lineages, at large exosomes could be creating a favored microenvironment to the journey of THCs through the circulation to organs they will later colonize.⁶⁰ Further research will be then needed to address those open questions.

As “white walkers,” THCs are literally a type of ‘Trojan horse’ cell that, with its defense system appearance, could convey tumor cells to remote sites to colonize other organs, avoiding immune system recognition. Our data reinforce the extremely complex concept of the metastatic pith and shed light on possible improvements in clinical practice to fight metastasis.

Acknowledgments

We thank Arturo Martínez-Arroyo for exosomes characterisation; Covadonga Aguado and Francisco Rafael Urbano for electron-

microscopy technical assistance; José Luis Martín-Ventura for LDL reagents; Daniel Pando for Transfectosome® technology; Ismael Morales-Flores for informatics support; María Elena Mansilla for karyotype assistance; Jose Casas, Aníbal Varela and Aurora Muñoz for technical assistance.

Disclosure of potential conflicts of interest

No potential conflicts of interest were disclosed.

Funding

Research in the laboratory of EL-C was supported by “Fundación para la Investigación Biomédica La Paz Hospital” (FIBHULP) and “Fundación Familia Alonso”.

Ethics approval and consent to participate

This study was approved by the Committee for Human Subjects of La Paz University Hospital (HULP: PI-3521) and the Clinical Research Ethics Committees of the Hospitals of Madrid (17.10.1125-GHM). Written informed consent was obtained from all participants. All animal studies were approved by the Ethics Committee for Animal Research from La Paz University Hospital (CSIC: 733/2018).

ORCID

Carlos del Fresno  <http://orcid.org/0000-0003-1771-7254>

References

- Siegel RL, Miller KD, Jemal A. Cancer statistics, 2016. *CA Cancer J Clin.* 2016;66:7–30. doi:10.3322/caac.21332.
- Reck M, Heigener DF, Mok T, Soria JC, Rabe KF. Management of non-small-cell lung cancer: recent developments. *Lancet.* 2013;382:709–719. doi:10.1016/S0140-6736(13)61502-0.
- Messaritakis I, Politaki E, Kotsakis A, Dermitzaki E-K, Koinis F, Lagoudaki E, Koutsopoulos A, Kallergi G, Souglakos J, Georgoulas V, et al. Phenotypic characterization of circulating tumor cells in the peripheral blood of patients with small cell lung cancer. *PLoS One.* 2017;12(7):e0181211. doi:10.1371/journal.pone.0181211.
- Jie XX, Zhang XY, Xu CJ. Epithelial-to-mesenchymal transition, circulating tumor cells and cancer metastasis: mechanisms and clinical applications. *Oncotarget.* 2017;8:81558–81571. doi:10.18632/oncotarget.18277.
- Massague J, Obenauf AC. Metastatic colonization by circulating tumour cells. *Nature.* 2016;529:298–306. doi:10.1038/nature17038.
- Azevedo AS, Follain G, Patthabhiraman S, Harlepp S, Goetz JG. Metastasis of circulating tumor cells: favorable soil or suitable biomechanics, or both? *Cell Adh Migr.* 2015;9:345–356. doi:10.1080/19336918.2015.1059563.
- Akhtar M, Haider A, Rashid S, Paget's A-NA. “Seed and soil” theory of cancer metastasis: an idea whose time has come. *Adv Anat Pathol.* 2019;26:69–74. doi:10.1097/PAP.0000000000000219.
- Merino D, Weber TS, Serrano A, Vaillant F, Liu K, Pal B, Di Stefano L, Schreuder J, Lin D, Chen Y, et al. Barcoding reveals complex clonal behavior in patient-derived xenografts of metastatic triple negative breast cancer. *Nat Commun.* 2019;10(1):766. doi:10.1038/s41467-019-08595-2.
- Klotz R, Thomas A, Teng T, Han SM, Iriondo O, Li L, Restrepo-Vassalli S, Wang A, Izadian N, MacKay M, et al. Circulating tumor cells exhibit metastatic tropism and reveal brain metastasis drivers. *Cancer Discov.* 2020 Jan;10(1):86–103. doi:10.1158/2159-8290.CD-19-0384
- Goldenberg DM, Pavia RA, Tsao MC. In vivo hybridisation of human tumour and normal hamster cells. *Nature.* 1974;250:649–651. doi:10.1038/250649a0.
- Pawelek JM. Tumour cell hybridization and metastasis revisited. *Melanoma Res.* 2000;10:507–514. doi:10.1097/00008390-200012000-00001.
- Gast CE, Silk AD, Zarour L, Riegler L, Burkhart JG, Gustafson KT, Parappilly MS, Roh-Johnson M, Goodman JR, Olson B, et al. Cell fusion potentiates tumor heterogeneity and reveals circulating hybrid cells that correlate with stage and survival. *Sci Adv.* 2018;4(9):eaat7828. doi:10.1126/sciadv.aat7828.
- Yilmaz Y, Lazova R, Qumsiyeh M, Cooper D, Pawelek J. Donor Y chromosome in renal carcinoma cells of a female BMT recipient: visualization of putative BMT-tumor hybrids by FISH. *Bone Marrow Transplant.* 2005;35:1021–1024. doi:10.1038/sj.bmt.1704939.
- Lazova R, Laberge GS, Duvall E, Spoelstra N, Klump V, Sznol M, Cooper D, Spritz RA, Chang JT, Pawelek JM, et al. A melanoma brain metastasis with a donor-patient hybrid genome following bone marrow transplantation: first evidence for fusion in human cancer. *PLoS One.* 2013;8(6):e66731. doi:10.1371/journal.pone.0066731.
- Chakraborty A, Lazova R, Davies S, Bäckvall H, Ponten F, Brash D, Pawelek J. Donor DNA in a renal cell carcinoma metastasis from a bone marrow transplant recipient. *Bone Marrow Transplantation.* 2004;34(2):183–186. doi:10.1038/sj.bmt.1704547.
- Pawelek JM, Chakraborty AK. Fusion of tumour cells with bone marrow-derived cells: a unifying explanation for metastasis. *Nat Rev Cancer.* 2008;8:377–386. doi:10.1038/nrc2371.
- Kerbel RS, Lagarde AE, Dennis JW, Donaghue TP. Spontaneous fusion in vivo between normal host and tumor cells: possible contribution to tumor progression and metastasis studied with a lectin-resistant mutant tumor. *Mol Cell Biol.* 1983;3:523–538. doi:10.1128/MCB.3.4.523.
- Busund LT, Killie MK, Bartnes K, Seljelid R. Spontaneously formed tumorigenic hybrids of Meth A sarcoma cells and macrophages in vivo. *Int J Cancer.* 2003;106:153–159. doi:10.1002/ijc.11210.
- Larizza L, Schirmacher V, Graf L, Pfluger E, Peres-Martinez M, Stohr M. Suggestive evidence that the highly metastatic variant ESb of the T-cell lymphoma Eb is derived from spontaneous fusion with a host macrophage. *Int J Cancer.* 1984;34:699–707. doi:10.1002/ijc.2910340518.
- Chakraborty AK, Sodi S, Rachkovsky M, Kolesnikova N, Platt JT, Bologna JL, Pawelek JM. A spontaneous murine melanoma lung metastasis comprised of host x tumor hybrids. *Cancer Res.* 2000;60:2512–2519.
- Noubissi FK, Harkness T, Alexander CM, Ogle BM. Apoptosis-induced cancer cell fusion: a mechanism of breast cancer metastasis. *Faseb J.* 2015;29:4036–4045. doi:10.1096/fj.15-271098.
- Lindstrom A, Midtbo K, Arnesson LG, Garvin S, Shabo I. Fusion between M2-macrophages and cancer cells results in a subpopulation of radioresistant cells with enhanced DNA-repair capacity. *Oncotarget.* 2017;8:51370–51386. doi:10.18632/oncotarget.17986.
- Zumsteg A, Baeriswyl V, Imaizumi N, Schwendener R, Ruegg C, Christofori G. Myeloid cells contribute to tumor lymphangiogenesis. *PLoS One.* 2009;4:e7067. doi:10.1371/journal.pone.0007067.
- Seyfried TN, Huysentruyt LC. On the origin of cancer metastasis. *Crit Rev Oncog.* 2013;18:43–73. doi:10.1615/CritRevOncog.v18.i1-2.40.
- Del Fresno C, Garcia-Rio F, Gomez-Pina V, Soares-Schanoski A, Fernández-Ruiz I, Jurado T, Kajiji T, Shu C, Marin E, Gutierrez Del Arroyo A, et al. Potent phagocytic activity with impaired antigen presentation identifying lipopolysaccharide-tolerant human monocytes: demonstration in isolated monocytes from cystic fibrosis patients. *J Immunol.* 2009;182(10):6494–6507. doi:10.4049/jimmunol.0803350.
- Lopez-Ayllon BD, Moncho-Amor V, Abarrategi A, de Cáceres II, Castro-Carpeño J, Belda-Iniesta C, Perona R, Sastre L. Cancer stem cells and cisplatin-resistant cells isolated from non-small-lung

- cancer cell lines constitute related cell populations. *Cancer Medicine*. 2014;3(5):1099–1111. doi:10.1002/cam4.291.
27. Ibrahim KE, Al-Mutary MG, Bakhiet AO, Khan HA. Histopathology of the liver, kidney, and spleen of mice exposed to gold nanoparticles. *Molecules*. 2018 Jul 25;23(8):1848.
 28. Kotecha N, Krutzik PO, Irish JM. Web-based analysis and publication of flow cytometry experiments. *Curr Protoc Cytom*. 2010 Chapter 10: Unit10 17;53(1):10.17.1–10.17.24. doi:10.1002/0471142956.cy1017s53.
 29. Rider MA, Hurwitz SN, Meckes DG Jr. ExtraPEG: A polyethylene glycol-based method for enrichment of extracellular vesicles. *Sci Rep*. 2016;6:23978. doi:10.1038/srep23978.
 30. Takahashi K, Yamanaka S. Induction of pluripotent stem cells from mouse embryonic and adult fibroblast cultures by defined factors. *Cell*. 2006;126:663–676. doi:10.1016/j.cell.2006.07.024.
 31. Boyette LB, Macedo C, Hadi K, Elinoff BD, Walters JT, Ramaswami B, Chalasani G, Taboas JM, Lakkis FG, Metes DM, et al. Phenotype, function, and differentiation potential of human monocyte subsets. *PLoS One*. 2017;12(4):e0176460. doi:10.1371/journal.pone.0176460.
 32. Wang P, Wan WW, Xiong SL, Feng H, Wu N. Cancer stem-like cells can be induced through dedifferentiation under hypoxic conditions in glioma, hepatoma and lung cancer. *Cell Death Discov*. 2017;3:16105. doi:10.1038/cddiscovery.2016.105.
 33. Zhao R, Chen M, Jiang Z, Zhao F, Xi B, Zhang X, Fu H, Zhou K. Platycodin-D induced autophagy in non-small cell lung cancer cells via PI3K/Akt/mTOR and MAPK signaling pathways. *J Cancer*. 2015;6(7):623–631. doi:10.7150/jca.11291.
 34. Sainz B Jr., Carron E, Vallespinos M, Machado HL. Cancer stem cells and macrophages: implications in tumor biology and therapeutic strategies. *Mediators Inflamm*. 2016;2016:9012369. doi:10.1155/2016/9012369.
 35. Pascual G, Avgustinova A, Mejetta S, Martín M, Castellanos A, Attolini CSO, Berenguer A, Prats N, Toll A, Huetto JA, et al. Targeting metastasis-initiating cells through the fatty acid receptor CD36. *Nature*. 2017;541(7635):41–45. doi:10.1038/nature20791.
 36. Vilahur G. New role for CD36 in metastasis through fat intake. *Cardiovasc Res*. 2017;113:e16–e17. doi:10.1093/cvr/cvx075.
 37. Helming L, Winter J, Gordon S. The scavenger receptor CD36 plays a role in cytokine-induced macrophage fusion. *J Cell Sci*. 2009;122:453–459. doi:10.1242/jcs.037200.
 38. Ishii T, Mann GE. Redox status in mammalian cells and stem cells during culture in vitro: critical roles of Nrf2 and cystine transporter activity in the maintenance of redox balance. *Redox Biol*. 2014;2:786–794. doi:10.1016/j.redox.2014.04.008.
 39. Hale JS, Otvos B, Sinyuk M, Alvarado AG, Hitomi M, Stoltz K, Wu Q, Flavahan W, Levison B, Johansen ML, et al. Cancer stem cell-specific scavenger receptor CD36 drives glioblastoma progression. *Stem Cells*. 2014;32(7):1746–1758. doi:10.1002/stem.1716.
 40. He C, Carter AB. The metabolic prospective and redox regulation of macrophage polarization. *J Clin Cell Immunol*. 2015;6(6):371.
 41. Colegio OR, Chu N-Q, Szabo AL, Chu T, Rhebergen AM, Jairam V, Cyrus N, Brokowski CE, Eisenbarth SC, Phillips GM, et al. Functional polarization of tumour-associated macrophages by tumour-derived lactic acid. *Nature*. 2014;513(7519):559–563. doi:10.1038/nature13490.
 42. Yoshida H, Kisugi R. Mechanisms of LDL oxidation. *Clin Chim Acta*. 2010;411:1875–1882. doi:10.1016/j.cca.2010.08.038.
 43. Seo JW, Yang EJ, Yoo KH, Choi IH. Macrophage differentiation from monocytes is influenced by the lipid oxidation degree of low density lipoprotein. *Mediators Inflamm*. 2015;2015:235797. doi:10.1155/2015/235797.
 44. Rattigan YI, Patel BB, Ackerstaff E, Sukenick G, Koutcher JA, Glod JW, Banerjee D. Lactate is a mediator of metabolic cooperation between stromal carcinoma associated fibroblasts and glycolytic tumor cells in the tumor microenvironment. *Exp Cell Res*. 2012;318(4):326–335. doi:10.1016/j.yexcr.2011.11.014.
 45. Clawson GA, Matters GL, Xin P, Imamura-Kawawasa Y, Du Z, Thiboutot DM, Helm KF, Neves RI, Abraham T. Macrophage-tumor cell fusions from peripheral blood of melanoma patients. *PLoS One*. 2015;10(8):e0134320. doi:10.1371/journal.pone.0134320.
 46. Ricciarelli R, Zingg JM, Azzi A. Vitamin E reduces the uptake of oxidized LDL by inhibiting CD36 scavenger receptor expression in cultured aortic smooth muscle cells. *Circulation*. 2000;102:82–87. doi:10.1161/01.CIR.102.1.82.
 47. Wong CW, Lee A, Shientag L, Yu J, Dong Y, Kao G, Al-Mehdi AB, Bernhard EJ, Muschel RJ. Apoptosis: an early event in metastatic inefficiency. *Cancer Res*. 2001;61:333–338.
 48. Krzewski K, Coligan JE. Human NK cell lytic granules and regulation of their exocytosis. *Front Immunol*. 2012;3:335. doi:10.3389/fimmu.2012.00335.
 49. Cubillos-Zapata C, Hernandez-Jimenez E, Avendano-Ortiz J, Toledano V, Varela-Serrano A, Fernández-Navarro I, Casitas R, Carpio C, Aguirre LA, García-Río F, et al. Obstructive sleep apnea monocytes exhibit high levels of vascular endothelial growth factor secretion, augmenting tumor progression. *Mediators Inflamm*. 2018;2018:7373921. doi:10.1155/2018/7373921.
 50. Wang H, Franco F, Tsui Y-C, Xie X, Trefny MP, Zappasodi R, Mohmood SR, Fernández-García J, Tsai C-H, Schulze I, et al. CD36-mediated metabolic adaptation supports regulatory T cell survival and function in tumors. *Nat Immunol*. 2020;21(3):298–308. doi:10.1038/s41590-019-0589-5.
 51. Welch DR, Hurst DR. Defining the hallmarks of metastasis. *Cancer Res*. 2019;79:3011–3027. doi:10.1158/0008-5472.CAN-19-0458.
 52. Hunter KW, Crawford NP, Alsarraj J. Mechanisms of metastasis. *Breast Cancer Res*. 2008;10(Suppl 1):S2. doi:10.1186/bcr1988.
 53. Stopeck AT, Lipton A, Body J-J, Steger GG, Tonkin K, de Boer RH, Lichinitser M, Fujiwara Y, Yardley DA, Viniegra M, et al. Denosumab compared with zoledronic acid for the treatment of bone metastases in patients with advanced breast cancer: a randomized, double-blind study. *J Clin Oncol*. 2010;28(35):5132–5139. doi:10.1200/JCO.2010.29.7101.
 54. Steger GG, Bartsch R. Denosumab for the treatment of bone metastases in breast cancer: evidence and opinion. *Ther Adv Med Oncol*. 2011;3(5):233–243. doi:10.1177/1758834011412656.
 55. Smith MR, Saad F, Oudard S, Shore N, Fizazi K, Sieber P, Tombal B, Damiao R, Marx G, Miller K, et al. Denosumab and bone metastasis-free survival in men with nonmetastatic castration-resistant prostate cancer: exploratory analyses by baseline prostate-specific antigen doubling time. *J Clin Oncol*. 2013;31(30):3800–3806. doi:10.1200/JCO.2012.44.6716.
 56. Kim M-Y, Oskarsson T, Acharyya S, Nguyen DX, Zhang XHF, Norton L, Massagué J. Tumor self-seeding by circulating cancer cells. *Cell*. 2009;139(7):1315–1326. doi:10.1016/j.cell.2009.11.025.
 57. Jia S, Zhang R, Li Z, Li J. Clinical and biological significance of circulating tumor cells, circulating tumor DNA, and exosomes as biomarkers in colorectal cancer. *Oncotarget*. 2017;8:55632–55645. doi:10.18632/oncotarget.17184.
 58. Clawson G. The fate of fusions. *Cells*. 2018;8(1):13.
 59. Manjunath Y, Porciani D, Mitchem JB, Suvilesh KN, Avella DM, Kimchi ET, Staveley-O'Carroll KF, Burke DH, Li G, Kaifi JT. Tumor-cell-macrophage fusion cells as liquid biomarkers and tumor enhancers in cancer. *Int J Mol Sci*. 2020;21(5):1872.
 60. Lobb RJ, Lima LG, Moller A. Exosomes: key mediators of metastasis and pre-metastatic niche formation. *Semin Cell Dev Biol*. 2017;67:3–10. doi:10.1016/j.semcdb.2017.01.004.